Electronic Supplementary Information for

Pyrazine Functionalization to Boost Antenna Effect in Rare Earth Metal-Organic Frameworks for Tetracyclines Detection

Kun Wu,[†a] Xin-Yi Liu,[†a] Yong-Liang Huang,[b] Mo Xie,[a] Xiao Xiong,[a] Ji Zheng,[a] Weigang Lu,*[a] and Dan Li*[a]

[a]College of Chemistry and Materials Science, Guangdong Provincial Key Laboratory of Functional Supramolecular Coordination Materials and Applications, Jinan University, Guangzhou, Guangdong 510632, P. R. China

[b]Department of Chemistry, Shantou University Medical College, Shantou, Guangdong 515041, P. R. China

† These authors contributed equally to this work.

E-mail: weiganglu@jnu.edu.cn, danli@jnu.edu.cn

Section 1. Synthesis of JNU-205-RE and JNU-206-RE

1.1. Materials and physical measurements

All reagents and materials were purchased commercially and used as received without further purification. $RE(NO_3)_2 \cdot 6H_2O$ and solvents were purchased from Energy Chemical, Shanghai tengzhun Biotechnology Co., Ltd, and Sigma-Aldrich Co., Inc. Fourier transform infrared (FT−IR) spectra were collected on a Thermo Scientific Nicolet iS10 spectrophotometer in the range of 4000−400 cm^{-1}. Powder X-ray diffraction (PXRD) was performed on Rigaku Ultima IV diffractometer (Cu Kα radiation, λ = 1.5406 Å). Single-crystal X-ray diffraction (SCXRD) data were collected at 100 K, via an Oxford Cryo stream system on a XtaLAB PRO MM007-DW diffractometer system equipped with a RA-Micro7HF-MR-DW(Cu/Mo) X-ray generator and HyPix-6000HE Hybrid Photon Counting (HPC) X-ray detector (Rigaku, Japan, Cu Kα, graphite monochromator, λ = 1.54 Å). CCDC-2142283-2142296 contain the supplementary crystallographic data for this paper. These data can be obtained free of charge from the Cambridge Crystallographic Data Centre www.ccdc.cam.ac.uk/structures. Thermogravimetric analysis (TGA) curves were obtained on Mettler-Toledo (TGA/DSC) thermal analyzer from 40 °C to 800 °C with a heating rate of 10 °C min^{-1} under a nitrogen gas atmosphere (20 mL·min^{-1}). Nitrogen gas adsorption/desorption measurements were performed on Micromeritics ASAP 2020 Plus adsorption instrument. Solid- and solution-state UV−Vis absorption spectra were recorded on Agilent Cary 4000. Cyclic voltammetry (CV) measurements were performed on a CHI 660E electrochemical workstation with a three-electrode cell in the supporting electrolyte. X-ray photoelectron spectroscopy (XPS) data were collected on a Thermo ESCALAB 250XI system. Solid- and solution-state luminescence spectra were measured on Horiba FluoroLog-3 spectrofluorometer.

1.2. Synthesis of H_4BTEB and H_4BTTB

H_4BTEB and H_4BTTB were synthesized according to literature reported method.[1-3]

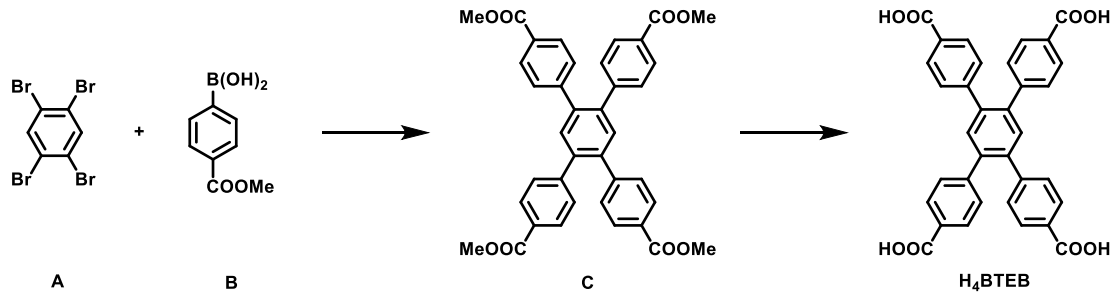

Fig. S1. The synthesis of **H4BTEB**.

Synthesis of **C**

To a solution of **A** (1.01 g, 2.54 mmol), **B** (2.42 g, 11.5 mol), [$Pd(PPh_3)_4$] (0.0881 g, 0.080 mmol), and K_3PO_4 (2.70 g, 12.70 mmol) in 250 mL of round bottom flask add 1,4-dioxane (100 mL), the resulting mixture was stirred for 96 h at 90 °C under N_2. After cooled down to room temperature, the reaction mixture was filtered, and the filtrate was evaporated, the residue was subjected to flash column chromatography of silica gel (petroleum ether : ethyl acetate = 4 : 1) to produce the intermediate **C** of 88% yield (1.25 g, 2.03 mmol). ^{1}H NMR (400 MHz, CD_2Cl_2) δ = 3.91 (12H, s), 7.34 (8H, dd), 7.62 (2H, s), 7.94 (8H, dd); ^{13}C NMR (100 MHz, CD_2Cl_2) δ = 67.0, 128.9, 129.3, 129.9, 132.7, 139.5, 144.9, 166.6.

Synthesis of **H4BTEB**

To a solution of **C** (2.0 g, 32.5 mmol) in THF/H_2O (1:1, 50 mL), add NaOH (2.0 g, 50. mmol), the resulting mixture was refluxed for 12 h. After cooled down to room temperature, THF was removed by rotary evaporator, and the remaining solution was acidified to pH = 3 with HCl (2.0 M). The precipitate was filtered and washed with distilled water to afford **H4BTEB** as a white solid (1.04 g, 1.87 mmol). ^{1}H NMR (400 MHz, DMSO-d_6) δ = 7.36 (8H, dd), 7.57 (2H, s), 7.84 (8H, dd), 12.99 (4H, s); ^{13}C NMR (100 MHz, DMSO-d_6) δ = 129.7, 129.9, 130.4, 139.4, 144.7, 167.5.

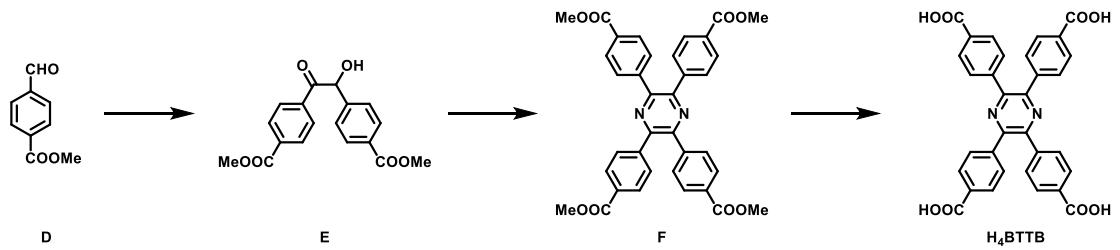

Fig. S2. The synthesis of **H_4BTTB**.

Synthesis of **E**

To a solution of VB_1 (6.0 g, 20 mmol) in a mixed solvent of CH_3OH (90 mL) and H_2O (30 mL), add NaOH (16.6 mL, 2 M) dropwise to adjust the pH to 9−10, then add **D** (50.0 g, 305 mmol). The resulting mixture was stirred for 1 h in ice bath, then it was heated at 60 °C for 1 h and at 85 °C for 3 h. The precipitate was filtered to produce **E**. ^{1}H NMR (400 MHz, $CDCl_3$): δ = 3.89 (3H, s), δ = 3.93 (3H, s), δ = 4.57 (1H, s), δ = 6.03 (1H, s), 7.42 (2H, dt), 7.94 (2H, dt), δ = 8.00 (2H, dt), δ = 8.07 (2H, dt); ^{13}C NMR (100 MHz, $CDCl_3$) δ =52.2, 52.7, 127.8, 128.9, 129.9, 130.5, 134.7, 136.6, 143.0, 165.8, 166.4, 198.3.

Synthesis of **F**

To a solution of **E** (30.1 g, 91.7 mmol) and CH_3COONH_4 (12 g, 155.7 mmol) in 90 mL of CH_3COOH, add acetic anhydride (9 mL, 91.7 mmol). After being stirred for 12 h at 120 °C under N_2, the dark orange precipitate was filtered and washed with diethyl ether to afford **F** (20.0 g, 32.5 mmol). ^{1}H NMR (400 MHz, $CDCl_3$): δ = 3.96 (12H, s), 7.71 (8H, dt), 8.03 (8H, dt); ^{13}C NMR (100 MHz, $CDCl_3$) δ =52.3, 129.7, 129.9, 130.6, 142.0, 148.3, 166.6.

Synthesis of **H_4BTTB**

To a solution of **F** (20.0 g, 32.5 mmol) in THF/H_2O (1:1, 250 mL), add NaOH (20.0 g, 500. mmol), the resulting mixture was refluxed for 12 h. THF was removed by rotary evaporator, and the remaining solution was acidified to pH = 3 with HCl (2.0 M). The precipitate was filtered and washed with distilled water to afford **H_4BTTB** as a light-yellow solid (16.18 g, 28.9 mmol). ^{1}H NMR (400 MHz, DMSO-d_6): δ = 7.67 (8H, dt), 7.94 (8H, dt); ^{13}C NMR (100 MHz, DMSO-d_6) δ =129.8, 130.4, 131.7, 142.8, 148.3, 167.4.

1.3. Synthesis of JNU-205-RE

JNU-205-Eu

A solution of $Eu(NO_3)_3·6H_2O$ (0.0336 mmol, 15 mg), H_4BTEB (0.0180 mmol, 10 mg), 2-fluorobenzoic acid (950 mg, 6.83 mmol), and *N,N*-dimethylformamide (DMF, 3 mL)

was added in a 10 mL glass vial, followed by heating at 120 ℃ for 72 h. After it was cooled to room temperature at a rate of 5 ℃/h, colorless hexagonal crystals of **JNU-205-Eu** were obtained in a yield of 55 % based on H_4BTEB.

JNU-205-Pr

A solution of **Pr** $(NO_3)_3 \cdot 6H_2O$ (0.0345 mmol, 15 mg), H_4BTEB (0.0180 mmol, 10 mg), 2-fluorobenzoic acid (950 mg, 6.78 mmol), and *N,N*-dimethylformamide (DMF, 3 mL) was added in a 10 mL glass vial, followed by heating at 120 ℃ for 72 h. After it was cooled to room temperature at a rate of 5 ℃/h, colorless hexagonal crystals of **JNU-205-Pr** were obtained in a yield of 36 % based on H_4BTEB.

JNU-205-Nd

A solution of $Nd(NO_3)_3 \cdot 6H_2O$ (0.0342 mmol, 15 mg), H_4BTEB (0.0180 mmol, 10 mg), 2-fluorobenzoic acid (850 mg, 6.07 mmol), and *N,N*-dimethylformamide (DMF, 3 mL) was added in a 10 mL glass vial, followed by heating at 120 ℃ for 72 h. After it was cooled to room temperature at a rate of 5 ℃/h, colorless hexagonal crystals of **JNU-205-Nd** were obtained in a yield of 61 % based on H_4BTEB.

JNU-205-Sm

A solution of $Sm(NO_3)_3 \cdot 6H_2O$ (0.0337 mmol, 15 mg), H_4BTEB (0.0176 mmol, 10 mg), 2-fluorobenzoic acid (850 mg, 6.07 mmol), and *N,N*-dimethylformamide (DMF, 3 mL) was added in a 10 mL glass vial, followed by heating at 120 ℃ for 72 h. After it was cooled to room temperature at a rate of 5 ℃/h, colorless hexagonal crystals of **JNU-206-Sm** were obtained in a yield of 56 % based on H_4BTTB.

JNU-205-Gd

A solution of $Gd(NO_3)_3 \cdot 6H_2O$ (0.0332 mmol, 15 mg), H_4BTEB (0.0180 mmol, 10 mg), 2-fluorobenzoic acid (950 mg, 6.78 mmol), and *N,N*-dimethylformamide (DMF, 3 mL) was added in a 10 mL glass vial, followed by heating at 120 ℃ for 72 h. After it was cooled to room temperature at a rate of 5 ℃/h, colorless hexagonal crystals of **JNU-205-Gd** were obtained in a yield of 49 % based on H_4BTEB.

JNU-205-Tb

A solution of $Tb(NO_3)_3 \cdot 6H_2O$ (0.0331 mmol, 15 mg), H_4BTEB (0.0180 mmol, 10 mg), 2-fluorobenzoic acid (850 mg, 6.07 mmol), and *N,N*-dimethylformamide (DMF, 3 mL) was added in a 10 mL glass vial, followed by heating at 120 ℃ for 72 h. After it was

cooled to room temperature at a rate of 5 ℃/h, colorless hexagonal crystals of **JNU-205-Tb** were obtained in a yield of 53 % based on H_4BTEB.

JNU-205-Dy

A solution of $Dy(NO_3)_3 \cdot 6H_2O$ (0.0329 mmol, 15 mg), H_4BTEB (0.0180 mmol, 10 mg), 2-fluorobenzoic acid (950 mg, 6.78 mmol), and *N,N*-dimethylformamide (DMF, 3 mL) was added in a 10 mL glass vial, followed by heating at 120 ℃ for 72 h. After it was cooled to room temperature at a rate of 5 ℃/h, colorless hexagonal crystals of **JNU-205-Dy** were obtained in a yield of 50 % based on H_4BTEB.

JNU-205-Ho

A solution of $Ho(NO_3)_3 \cdot 6H_2O$ (0.0327 mmol, 15 mg), H_4BTEB (0.0180 mmol, 10 mg), 2-fluorobenzoic acid (950 mg, 6.78 mmol), and *N,N*-dimethylformamide (DMF, 3 mL) was added in a 10 mL glass vial, followed by heating at 120 ℃ for 72 h. After it was cooled to room temperature at a rate of 5 ℃/h, colorless hexagonal crystals of **JNU-205-Ho** were obtained in a yield of 55 % based on H_4BTEB.

JNU-205-Er

A solution of $Er(NO_3)_3 \cdot 6H_2O$ (0.0332 mmol, 15 mg), H_4BTEB (0.0180 mmol, 10 mg), 2-fluorobenzoic acid (950 mg, 6.78 mmol), and *N,N*-dimethylformamide (DMF, 3 mL) was added in a 10 mL glass vial, followed by heating at 120 ℃ for 72 h. After it was cooled to room temperature at a rate of 5 ℃/h, colorless hexagonal crystals of **JNU-205-Er** were obtained in a yield of 59 % based on H_4BTEB.

JNU-205-Tm

A solution of $Tm(NO_3)_3 \cdot 6H_2O$ (0.0324 mmol, 15 mg), H_4BTEB (0.0180 mmol, 10 mg), 2-fluorobenzoic acid (850 mg, 6.07 mmol), and *N,N*-dimethylformamide (DMF, 3 mL) was added in a 10 mL glass vial, followed by heating at 120 ℃ for 72 h. After it was cooled to room temperature at a rate of 5 ℃/h, colorless hexagonal crystals of **JNU-205-Tm** were obtained in a yield of 47 % based on H_4BTEB.

JNU-205-Yb

A solution of $Yb(NO_3)_3 \cdot 6H_2O$ (0.0334 mmol, 15 mg), H_4BTEB (0.0180 mmol, 10 mg), 2-fluorobenzoic acid (950 mg, 6.78 mmol), and *N,N*-dimethylformamide (DMF, 3 mL) was added in a 10 mL glass vial, followed by heating at 120 ℃ for 72 h. After it was cooled to room temperature at a rate of 5 ℃/h, colorless hexagonal crystals of **JNU-**

205-Yb were obtained in a yield of 52 % based on H_4BTEB.

JNU-205-Lu

A solution of $Lu(NO_3)_3 \cdot 6H_2O$ (0.0346 mmol, 15 mg), H_4BTEB (0.0180 mmol, 10 mg), 2-fluorobenzoic acid (1150 mg, 8.21mmol), and *N,N*-dimethylformamide (DMF, 3 mL) was added in a 10 mL glass vial, followed by heating at 120 ℃ for 72 h. After it was cooled to room temperature at a rate of 5 ℃/h, colorless hexagonal crystals of **JNU-205-Lu** were obtained in a yield of 60 % based on H_4BTEB.

JNU-205-Y

A solution of $Y(NO_3)_3 \cdot 6H_2O$ (0.0392 mmol, 15 mg), H_4BTEB (0.0180 mmol, 10 mg), 2-fluorobenzoic acid (950 mg, 6.78mmol), and *N,N*-dimethylformamide (DMF, 3 mL) was added in a 10 mL glass vial, followed by heating at 120 ℃ for 72 h. After it was cooled to room temperature at a rate of 5 ℃/h, colorless hexagonal crystals of **JNU-205-Y** were obtained in a yield of 51 % based on H_4BTEB.

1.4. Syntheses of JNU-206-RE

JNU-206-Eu

A solution of $Eu(NO_3)_3 \cdot 6H_2O$ (0.0336 mmol, 15 mg), H_4BTTB (0.0176 mmol, 10 mg), 2-fluorobenzoic acid (650 mg, 4.67 mmol), and *N,N*-dimethylformamide (DMF, 3 mL) was added in a 10 mL glass vial, followed by heating at 120 ℃ for 72 h. After it was cooled to room temperature at a rate of 5 ℃/h, colorless hexagonal crystals of **JNU-206-Eu** were obtained in a yield of 56 % based on H_4BTTB. IR (KBr): 3394 (br, s), 1593 (s), 1540 (s), 1405 (m), 1306 (w), 1181 (w), 1146 (w), 1103 (w), 1045 (s), 1016 (m), 859 (w), 789 (m), 715 (m), 571 (w), 494 (w) cm^{-1}.

JNU-206-Pr

A solution of $Pr(NO_3)_3 \cdot 6H_2O$ (0.0345 mmol, 15 mg), H_4BTTB (0.0176 mmol, 10 mg), 2-fluorobenzoic acid (450 mg, 3.24 mmol), and *N,N*-dimethylformamide (DMF, 3 mL) was added in a 10 mL glass vial, followed by heating at 120 ℃ for 72 h. After it was cooled to room temperature at a rate of 5 ℃/h, colorless hexagonal crystals of **JNU-206-Pr** were obtained in a yield of 43 % based on H_4BTTB. IR (KBr): 3365 (br, s), 1658 (w), 1598(s), 1557 (w), 1404 (s), 1317 (w), 1096 (w), 1012 (s), 863 (w), 791 (s), 697 (w), 661 (w), 575 (w) cm^{-1}.

JNU-206-Nd

A solution of $Nd(NO_3)_3 \cdot 6H_2O$ (0.0342 mmol, 15 mg), H_4BTTB (0.0176 mmol, 10 mg), 2-fluorobenzoic acid (550 mg, 3.95 mmol), and *N,N*-dimethylformamide (DMF, 3 mL) was added in a 10 mL glass vial, followed by heating at 120 ℃ for 72 h. After it was cooled to room temperature at a rate of 5 ℃/h, colorless hexagonal crystals of **JNU-206-Nd** were obtained in a yield of 53 % based on H_4BTTB. IR (KBr): 3361 (br, s), 1656 (m), 1598 (s), 1548 (m), 1404 (m), 1178 (w), 1144 (w), 1096 (s), 1011 (s), 863 (s), 790 (s), 759 (s), 715 (m), 661 (m) cm^{-1}.

JNU-206-Sm

A solution of $Sm(NO_3)_3 \cdot 6H_2O$ (0.0337 mmol, 15 mg), H_4BTTB (0.0176 mmol, 10 mg), 2-fluorobenzoic acid (550 mg, 3.95 mmol), and *N,N*-dimethylformamide (DMF, 3 mL) was added in a 10 mL glass vial, followed by heating at 120 ℃ for 72 h. After it was cooled to room temperature at a rate of 5 ℃/h, colorless hexagonal crystals of **JNU-206-Sm** were obtained in a yield of 60 % based on H_4BTTB. IR (KBr): 3377 (br, s), 1656 (m), 1590 (s), 1541 (m), 1386 (m), 1178 (w), 1144 (w), 1103 (s), 1011 (s), 857 (s), 787 (s), 712 (s), 675 (m), 555 (m) cm^{-1}.

JNU-206-Gd

A solution of $Gd(NO_3)_3 \cdot 6H_2O$ (0.0332 mmol, 15 mg), H_4BTTB (0.0176 mmol, 10 mg), 2-fluorobenzoic acid (750 mg, 5.39 mmol), and *N,N*-dimethylformamide (DMF, 3 mL) was added in a 10 mL glass vial, followed by heating at 120 ℃ for 72 h. After it was cooled to room temperature at a rate of 5 ℃/h, colorless hexagonal crystals of **JNU-206-Gd** were obtained in a yield of 49 % based on H_4BTTB. IR (KBr): 3344 (br, s), 1660 (m), 1602 (s), 1549 (m), 1406 (w), 1180 (w), 1146 (w), 1100 (m), 1012 (s), 965 (w), 859 (w), 790 (s), 714 (w), 575 (w) cm^{-1}.

JNU-206-Tb

A solution of $Tb(NO_3)_3 \cdot 6H_2O$ (0.0331 mmol, 15 mg), H_4BTTB (0.0176 mmol, 10 mg), 2-fluorobenzoic acid (750 mg, 5.39 mmol), and *N,N*-dimethylformamide (DMF, 3 mL) was added in a 10 mL glass vial, followed by heating at 120 ℃ for 72 h. After it was cooled to room temperature at a rate of 5 ℃/h, colorless hexagonal crystals of **JNU-206-Tb** were obtained in a yield of 60 % based on H_4BTTB. IR (KBr): 3354 (br, s),

1656 (s), 1594 (s), 1544 (s), 1387 (m), 1179 (w), 1145 (w), 1101 (s), 1011 (s), 863 (w), 789 (s), 714 (w), 572 (w), 490 (w) cm^{-1}.

JNU-206-Dy

A solution of $Dy(NO_3)_3 \cdot 6H_2O$ (0.0329 mmol, 15 mg), H_4BTTB (0.0176 mmol, 10 mg), 2-fluorobenzoic acid (650 mg, 4.67 mmol), and *N,N*-dimethylformamide (DMF, 3 mL) was added in a 10 mL glass vial, followed by heating at 120 ℃ for 72 h. After it was cooled to room temperature at a rate of 5 ℃/h, colorless hexagonal crystals of **JNU-206-Dy** were obtained in a yield of 56 % based on H_4BTTB. IR (KBr): 3362 (br, s), 1656 (m), 1590 (s), 1541 (m), 1386 (w), 1179 (w), 1146 (w), 1100 (m), 1011 (s), 862 (w), 788 (s), 714 (w), 561 (w) cm^{-1}.

JNU-206-Ho

A solution of $Ho(NO_3)_3 \cdot 6H_2O$ (0.0327 mmol, 15 mg), H_4BTTB (0.0176 mmol, 10 mg), 2-fluorobenzoic acid (850 mg, 6.11 mmol), and *N,N*-dimethylformamide (DMF, 3 mL) was added in a 10 mL glass vial, followed by heating at 120 ℃ for 72 h. After it was cooled to room temperature at a rate of 5 ℃/h, colorless hexagonal crystals of **JNU-206-Ho** were obtained in a yield of 59 % based on H_4BTTB. IR (KBr): 3343 (br, s), 1656 (m), 1590 (s), 1542 (m), 1386 (w), 1179 (w), 1145 (w), 1105 (m), 1011 (s), 862 (w), 788 (s), 714 (w), 678 (w), 572 (w) cm^{-1}.

JNU-206-Er

A solution of $Er(NO_3)_3 \cdot 6H_2O$ (0.0332 mmol, 15 mg), H_4BTTB (0.0176 mmol, 10 mg), 2-fluorobenzoic acid (650 mg, 4.67 mmol), and *N,N*-dimethylformamide (DMF, 3 mL) was added in a 10 mL glass vial, followed by heating at 120 ℃ for 72 h. After it was cooled to room temperature at a rate of 5 ℃/h, colorless hexagonal crystals of **JNU-206-Er** were obtained in a yield of 49 % based on H_4BTTB. IR (KBr): 3325 (br, s), 1660 (m), 1693 (s), 1544 (m), 1386 (w), 1178 (w), 1145 (w), 1097 (m), 1011 (s), 863 (w), 787 (s), 713(w), 565 (w) cm^{-1}.

JNU-206-Tm

A solution of $Tm(NO_3)_3 \cdot 6H_2O$ (0.0324 mmol, 15 mg), H_4BTTB (0.0176 mmol, 10 mg), 2-fluorobenzoic acid (650 mg, 4.67 mmol), and *N,N*-dimethylformamide (DMF, 3 mL) was added in a 10 mL glass vial, followed by heating at 120 ℃ for 72 h., After it was

cooled to room temperature at a rate of 5 ℃/h, colorless hexagonal crystals of **JNU-206-Tm** were obtained in a yield of 53 % based on H_4BTTB. IR (KBr): 3344 (br, s), 1659 (s), 1592 (s), 1544 (m), 1386 (w), 1179 (w), 1146 (w), 1097 (m), 1011 (s), 863 (w), 787 (s), 713 (w), 562 (w) cm^{-1}.

JNU-206-Yb

A solution of $Yb(NO_3)_3 \cdot 6H_2O$ (0.0334 mmol, 15 mg), H_4BTTB (0.0176 mmol, 10 mg), 2-fluorobenzoic acid (650 mg, 4.67 mmol), and *N,N*-dimethylformamide (DMF, 3 mL) was added in a 10 mL glass vial, followed by heating at 120 ℃ for 72 h. After it was cooled to room temperature at a rate of 5 ℃/h, colorless hexagonal crystals of **JNU-206-Yb** were obtained in a yield of 61 % based on H_4BTTB. IR (KBr): 3392 (br, s), 1659 (m), 1592 (s), 1544 (m), 1386 (w), 1178 (w), 1099 (m), 1011 (s), 865 (s), 788 (s), 713 (w), 576 (w) cm^{-1}.

JNU-206-Lu

A solution of $Lu(NO_3)_3 \cdot 6H_2O$ (0.0346 mmol, 15 mg), H_4BTTB (0.0176 mmol, 10 mg), 2-fluorobenzoic acid (650 mg, 4.67 mmol), and *N,N*-dimethylformamide (DMF, 3 mL) was added in a 10 mL glass vial, followed by heating at 120 ℃ for 72 h. After it was cooled to room temperature at a rate of 5 ℃/h, colorless hexagonal crystals of **JNU-206-Lu** were obtained in a yield of 60 % based on H_4BTTB. IR (KBr): 3350 (br, s), 1660 (m), 1594 (s), 1545 (m), 1178 (w), 1146 (w), 1097 (m), 1011 (s), 864 (w), 787 (s), 713 (w), 572 (w) cm^{-1}.

JNU-206-Y

A solution of $Y(NO_3)_3 \cdot 6H_2O$ (0.0392 mmol, 15 mg), H_4BTTB (0.0176 mmol, 10 mg), 2-fluorobenzoic acid (600 mg, 4.31mmol), and *N,N*-dimethylformamide (DMF, 3 mL) was added in a 10 mL glass vial, followed by heating at 120 ℃ for 72 h. After it was cooled to room temperature at a rate of 5 ℃/h, colorless hexagonal crystals of **JNU-206-Y** were obtained in a yield of 48% based on H_4BTTB. IR (KBr): 3351 (br, s), 1659 (s), 15966 (s), 1541 (s), 1405 (m), 1178 (m), 1144 (w), 1102 (s), 1011 (s), 862 (m), 789 (s), 714 (w), 559 (w), 491 (w) cm^{-1}.

Section 2. Characterization of JNU-205-RE and JNU-206-RE

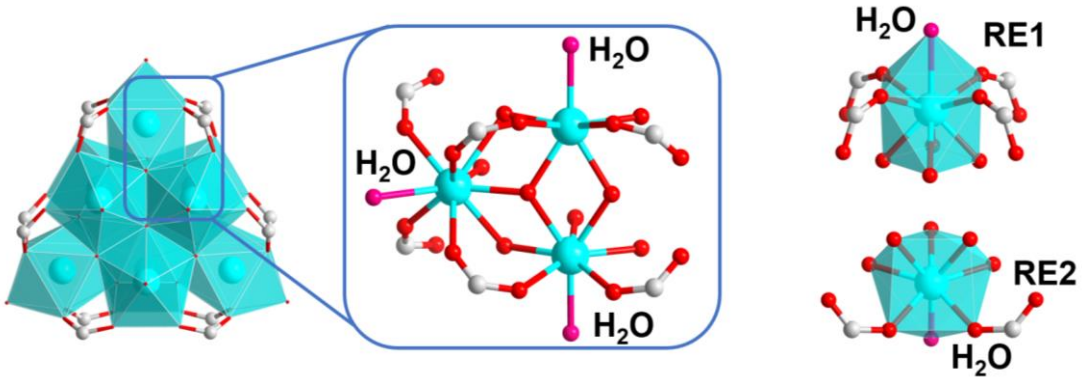

Fig. S3. Local coordination environment of RE1 and RE2.

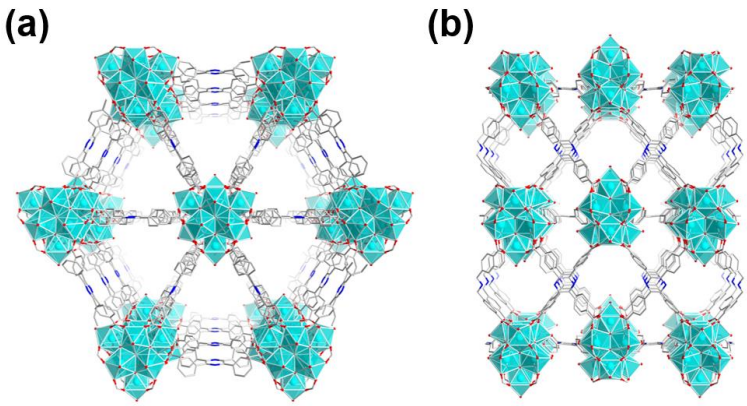

Fig. S4. Ball-and-stick model of the **JNU-206-RE** along (a) a and (b) c directions. (sky blue for RE, red for O, gray for C and blue for N, H atoms are omitted for clarity).

2.1 Crystal structure of JNU-205-RE

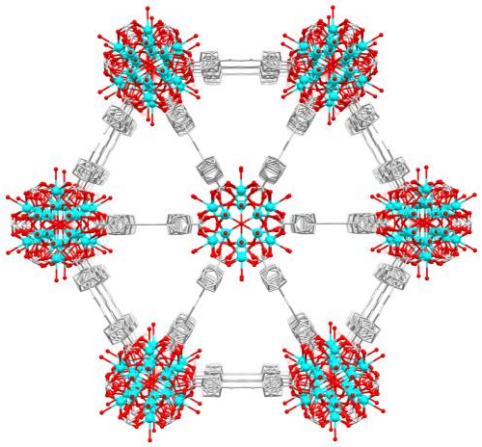

Fig. S5. Crystal structure of **JNU-205-Eu** viewed along [001] direction.

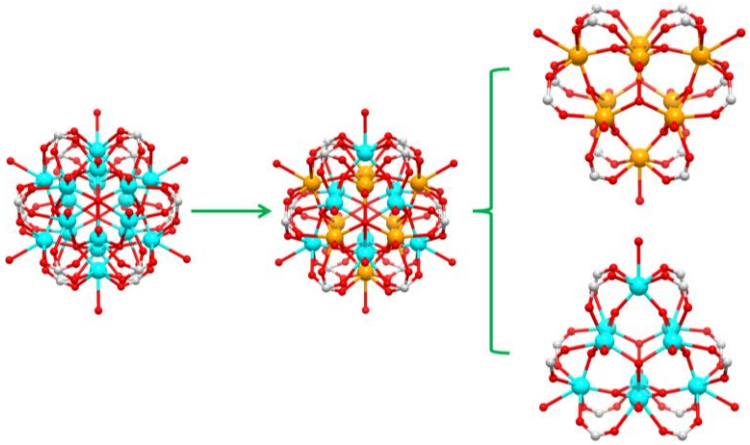

Fig. S6. The disorder of the Eu_9-cluster with two sets of orientations in **JNU-205-Eu** (light orange and turquoise).

2.2 Crystal structure of JNU-206-RE

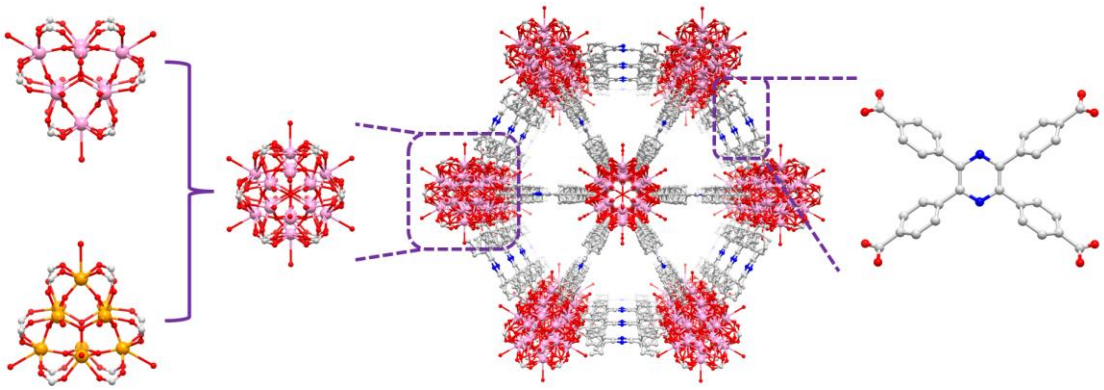

Fig. S7. View of **JNU-206-Pr** along the [001] direction with uniformed triangular 1D channels (colour code: C, gray; N, blue; O, red; and Pr, rose/light orange. H atoms are omitted for clarity).

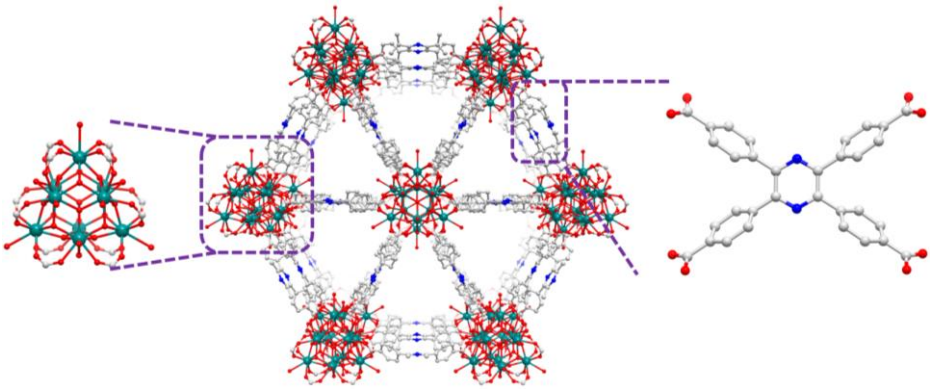

Fig. S8. View of **JNU-206-Nd** along the [001] direction with uniformed triangular 1D

channels (colour code: C, gray; N, blue; O, red; and Nd, teal. H atoms are omitted for clarity).

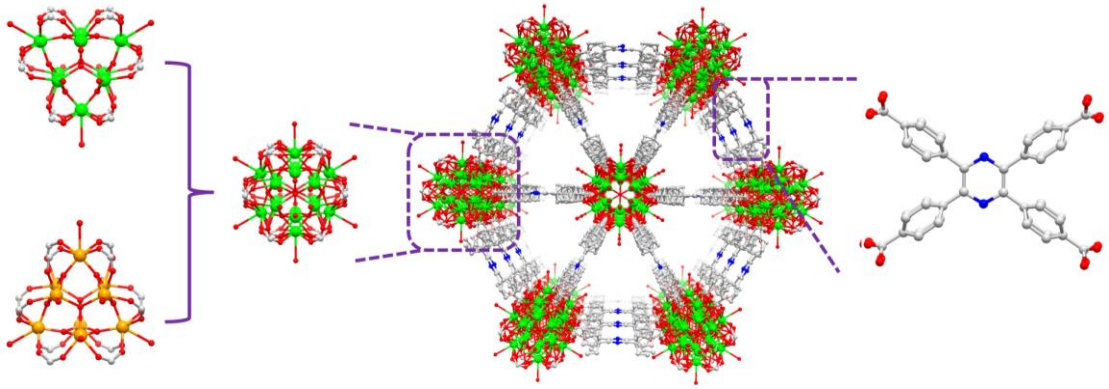

Fig. S9. Views of **JNU-206-Sm** along the [001] direction with uniformed triangular 1D channels (colour code: C, gray; N, blue; O, red; and Sm, bright green/light orange. H atoms are omitted for clarity).

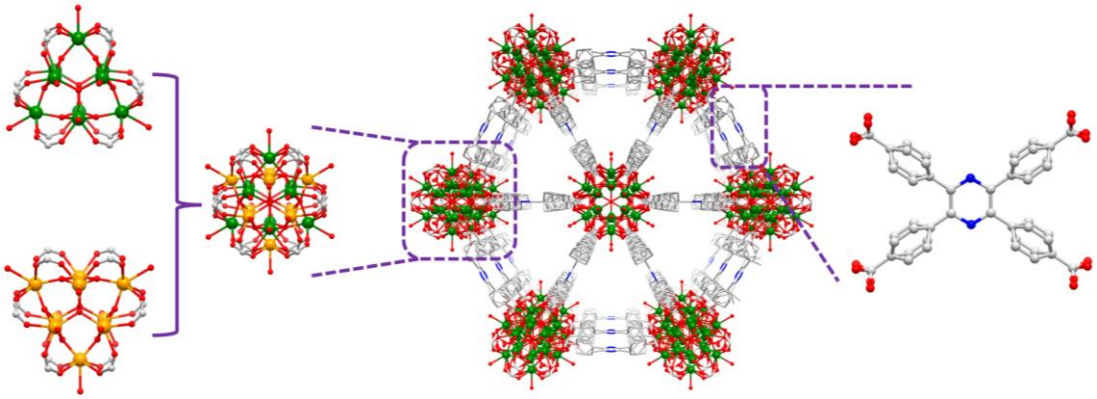

Fig. S10. Views of **JNU-206-Gd** along the [001] direction with uniformed triangular 1D channels (colour code: C, gray; N, blue; O, red; and Gd, green/light orange. H atoms are omitted for clarity).

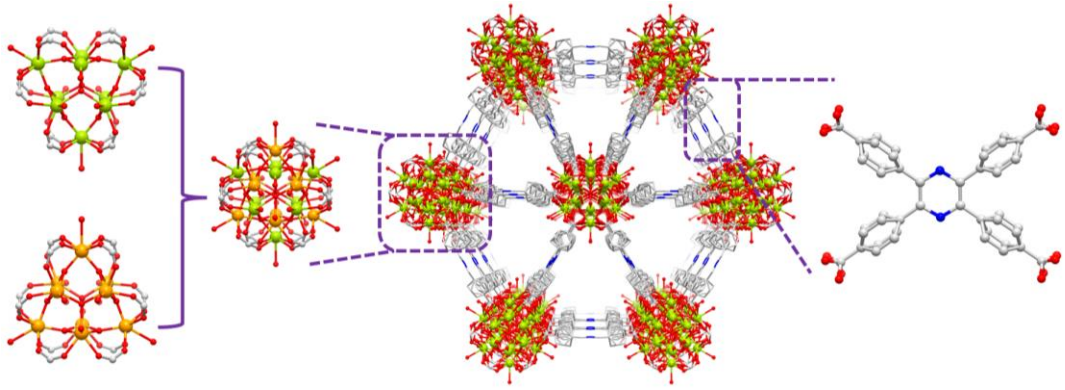

Fig. S11. Views of **JNU-206-Tb** along the [001] direction with uniformed triangular 1D channels (colour code: C, gray; N, blue; O, red; and Tb, lime/light orange. H atoms are omitted for clarity).

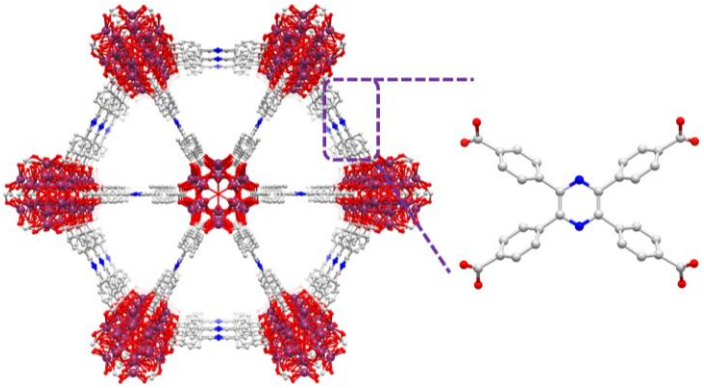

Fig. S12. Views of **JNU-206-Ho** along the [001] direction with uniformed triangular 1D channels (colour code: C, gray; N, blue; O, red; and Ho, plum. H atoms are omitted for clarity).

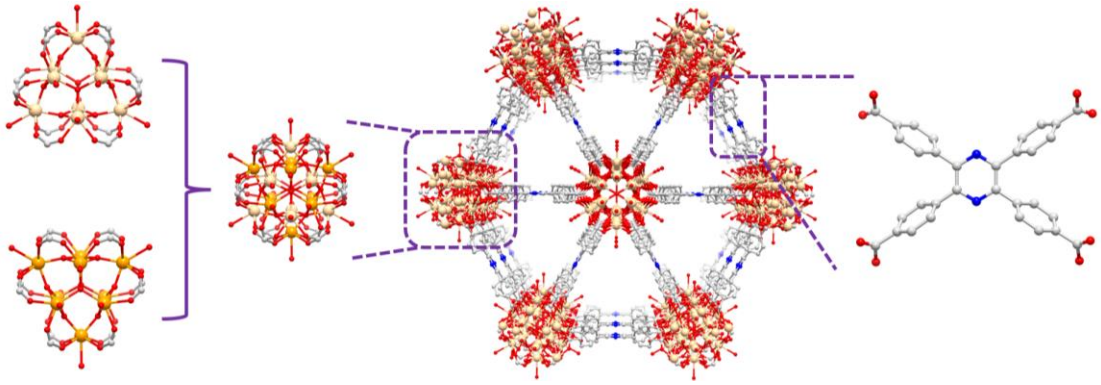

Fig. S13. Views of **JNU-206-Dy** along the [001] direction with uniformed triangular 1D channels (colour code: C, gray; N, blue; O, red; and Dy, tan/light orange. H atoms are omitted for clarity).

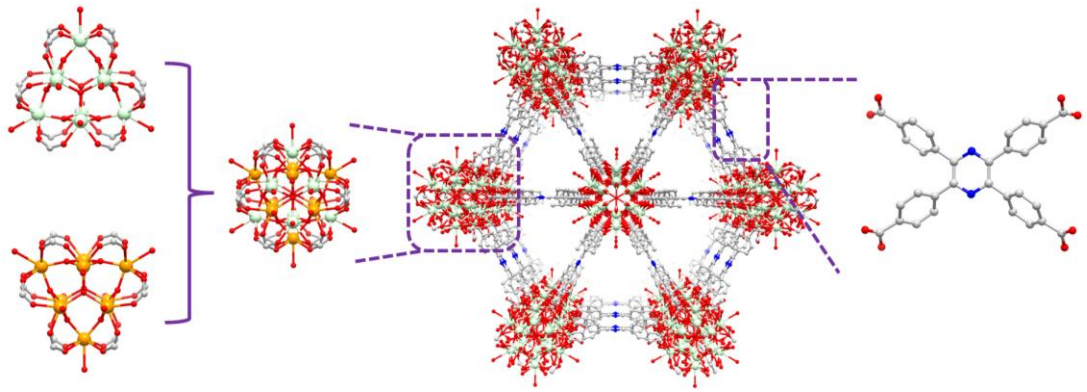

Fig. S14. Views of **JNU-206-Er** along the [001] direction with uniformed triangular 1D channels (colour code: C, gray; N, blue; O, red; and Er, light green/light orange. H atoms are omitted for clarity).

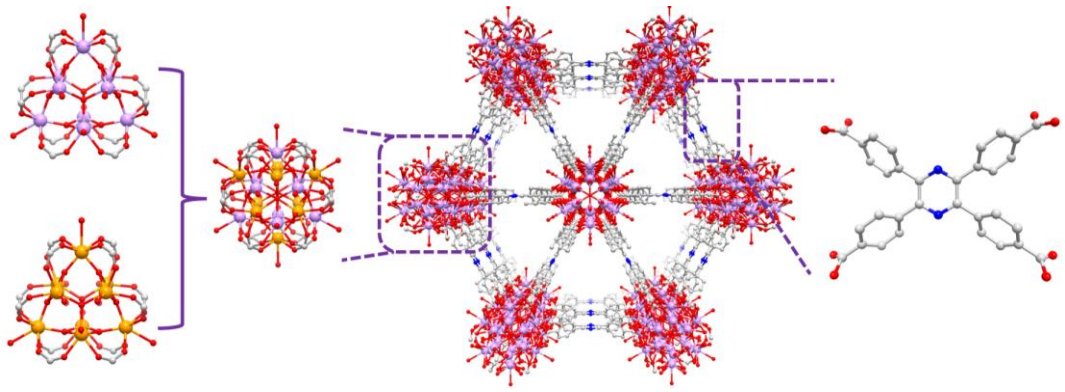

Fig. S15. Views of **JNU-206-Tm** along the [001] direction with uniformed triangular 1D channels (colour code: C, gray; N, blue; O, red; and Tm, lavender/light orange. H atoms are omitted for clarity).

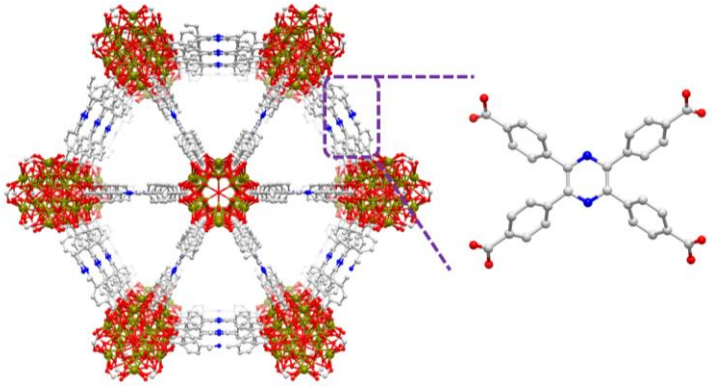

Fig. S16. Views of **JNU-206-Yb** along the [001] direction with uniformed triangular 1D channels (colour code: C, gray; N, blue; O, red; and Yb, dark yellow. H atoms are

omitted for clarity).

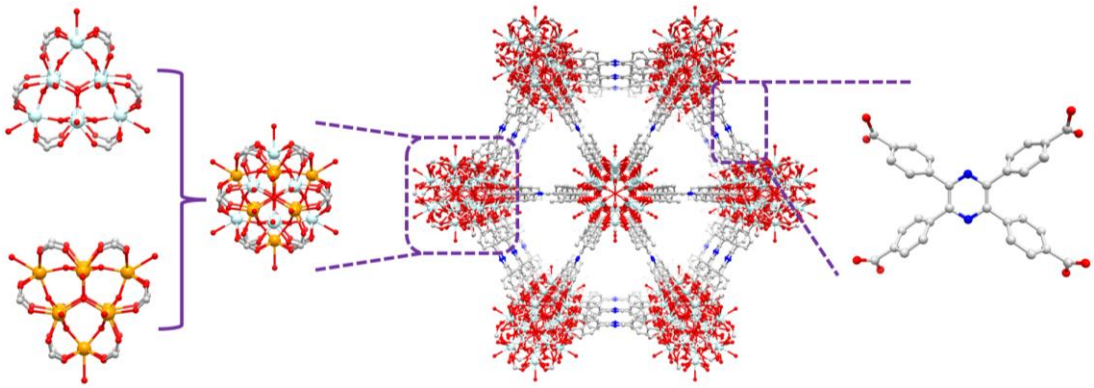

Fig. S17. Views of **JNU-206-Lu** along the [001] direction with uniformed triangular 1D channels (colour code: C, gray; N, blue; O, red; and Lu, light turquoise/light orange. H atoms are omitted for clarity).

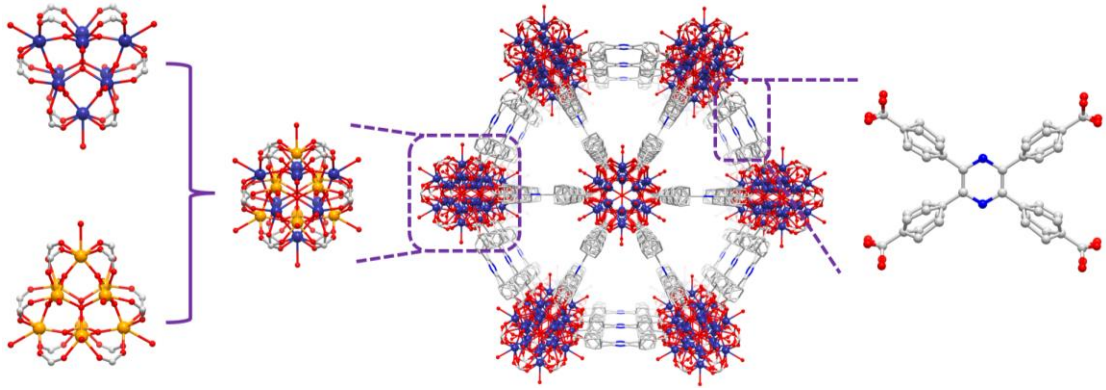

Fig. S18. Views of **JNU-206-Y** along the [001] direction with uniformed triangular 1D channels (colour code: C, gray; N, blue; O, red; and Y, indigo/light orange. H atoms are omitted for clarity).

2.3 Desktop SEM images of JNU-205-RE

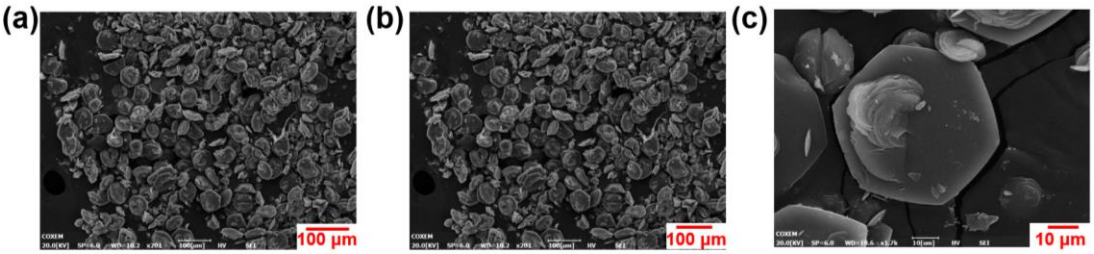

Fig. S19. SEM image of **JNU-205-Eu**.

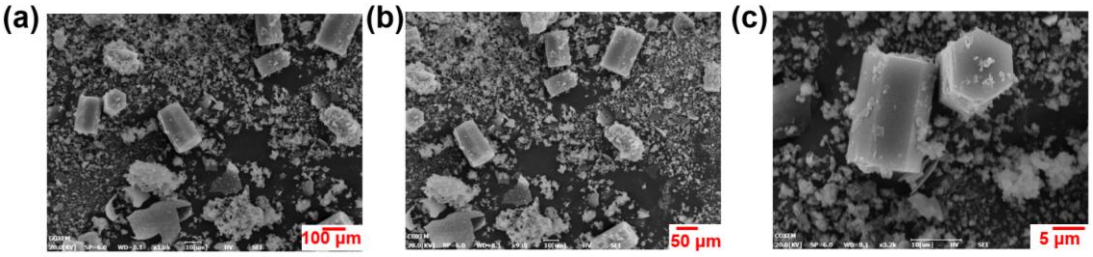

Fig. S20. SEM image of **JNU-205-Eu**.

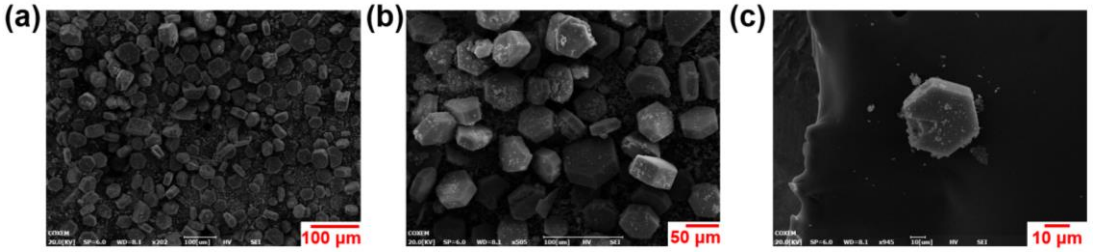

Fig. S21. SEM image of **JNU-205-Nd**.

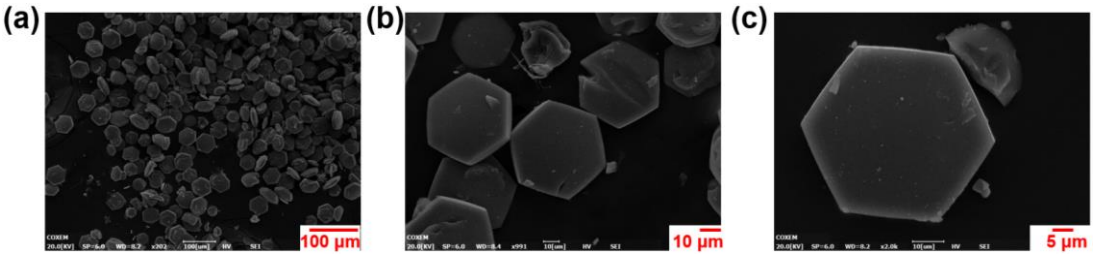

Fig. S22. SEM image of **JNU-205-Sm**.

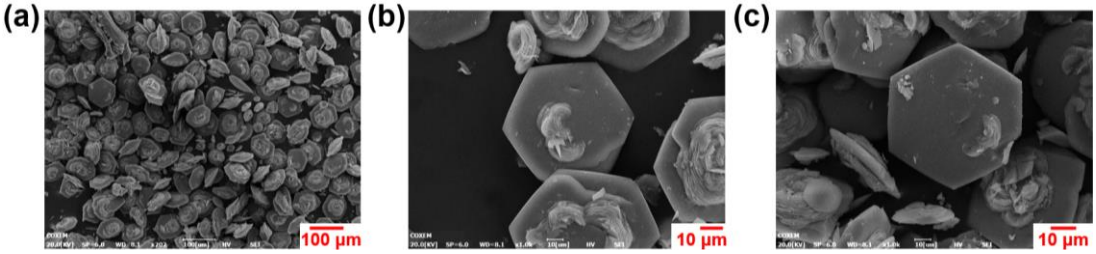

Fig. S23. SEM image of **JNU-205-Gd**.

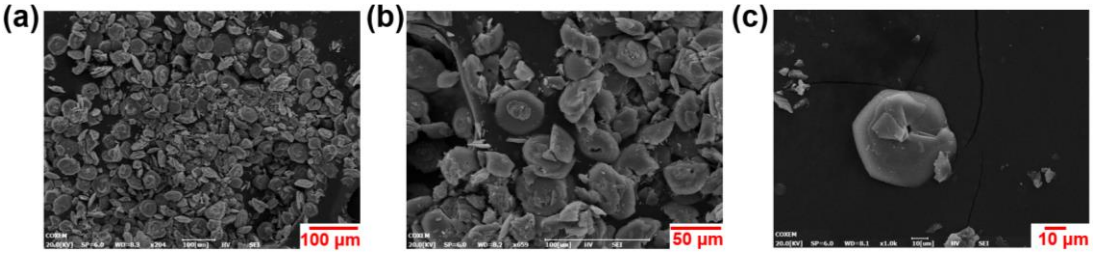

Fig. S24. SEM image of **JNU-205-Tb**.

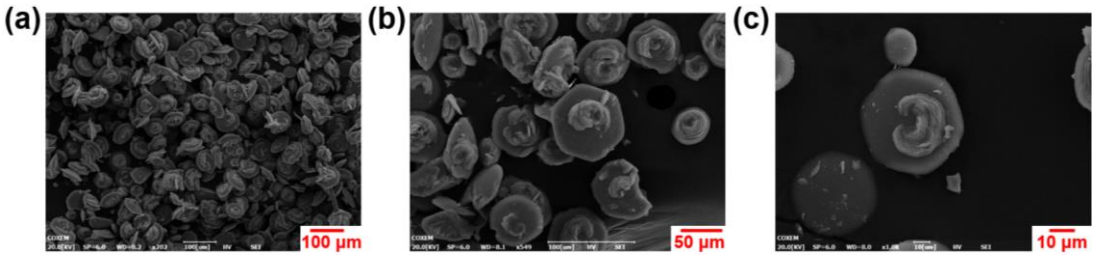

Fig. S25. SEM image of **JNU-205-Dy**.

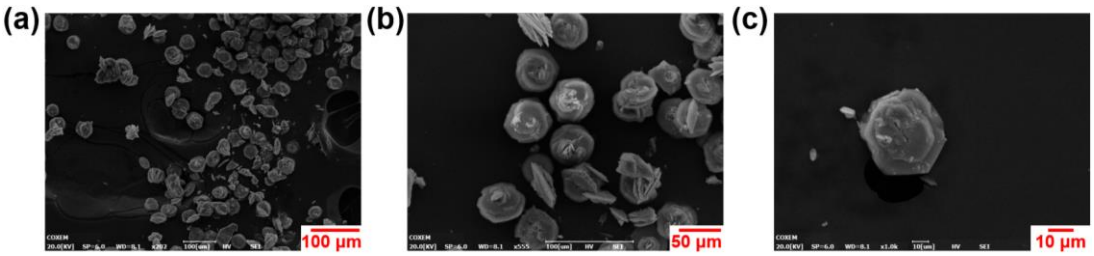

Fig. S26. SEM image of **JNU-205-Ho**.

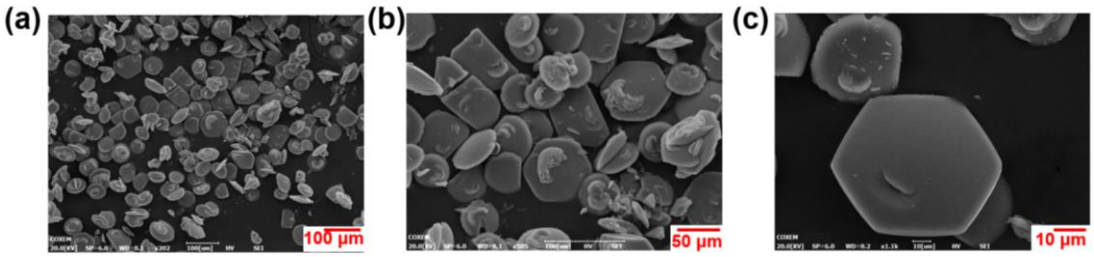

Fig. S27. SEM image of **JNU-205-Er**.

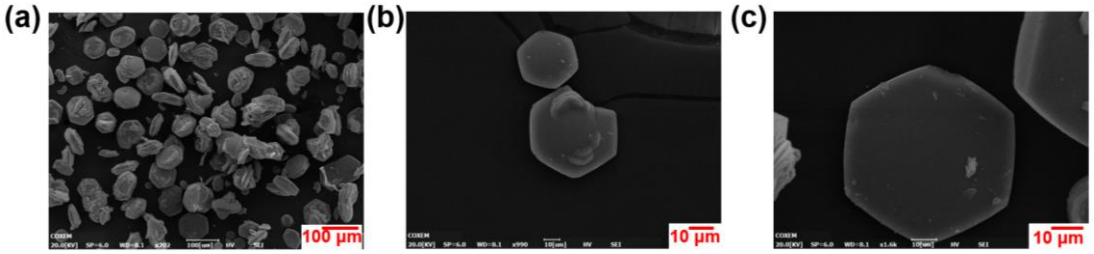

Fig. S28. SEM image of **JNU-205-Tm**.

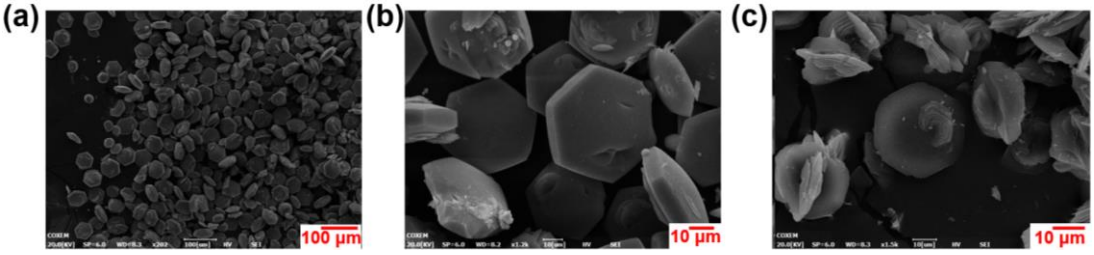

Fig. S29. SEM image of **JNU-205-Yb**.

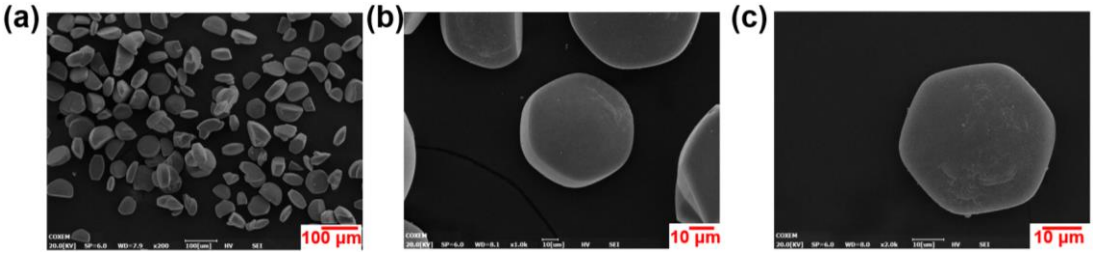

Fig. S30. SEM image of **JNU-205-Lu**.

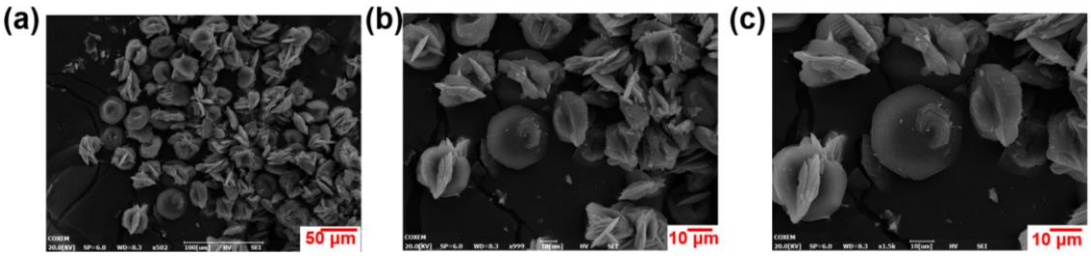

Fig. S31. SEM image of **JNU-205-Y**.

2.4 Desktop SEM images of JNU-206-RE

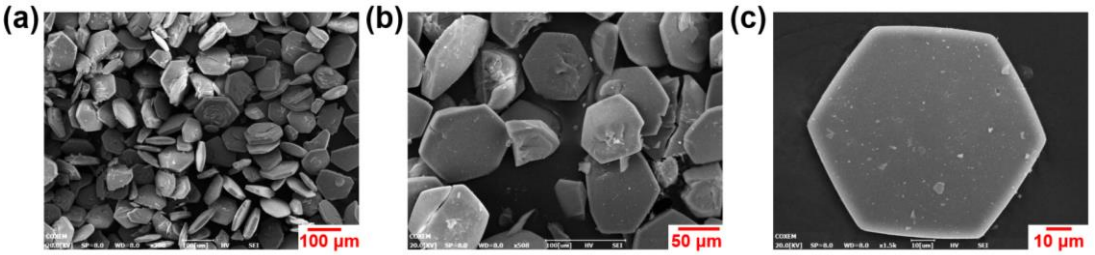

Fig. S32. SEM image of **JNU-206-Eu**.

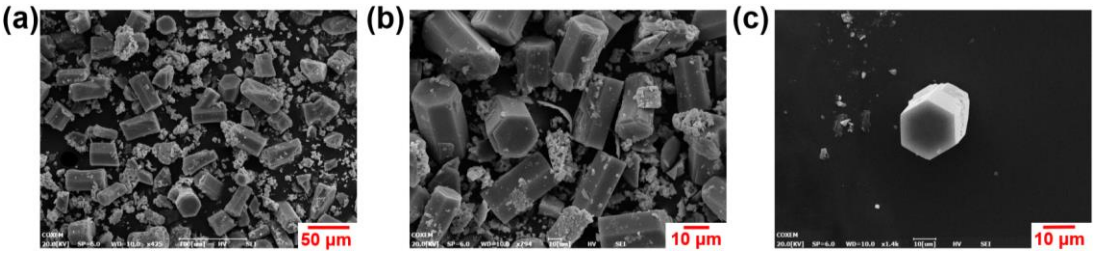

Fig. S33. SEM image of **JNU-206-Pr**.

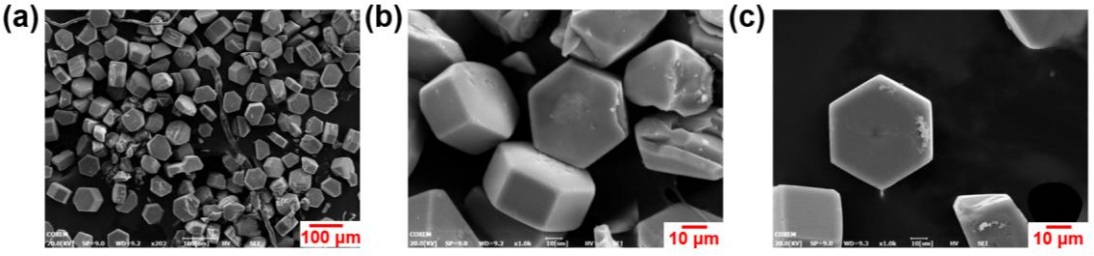

Fig. S34. SEM image of **JNU-206-Nd**.

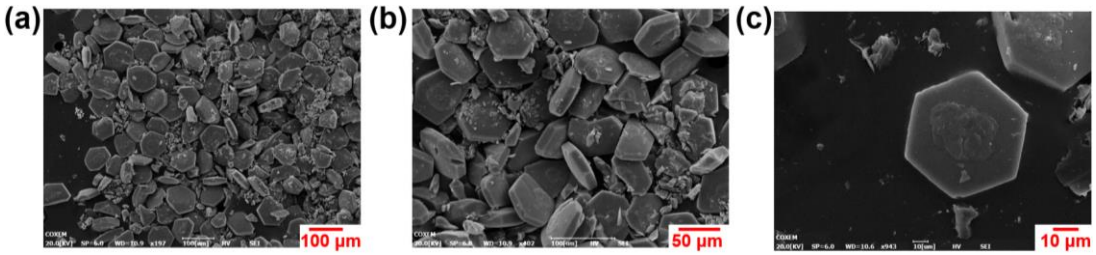

Fig. S35. SEM image of **JNU-206-Sm**.

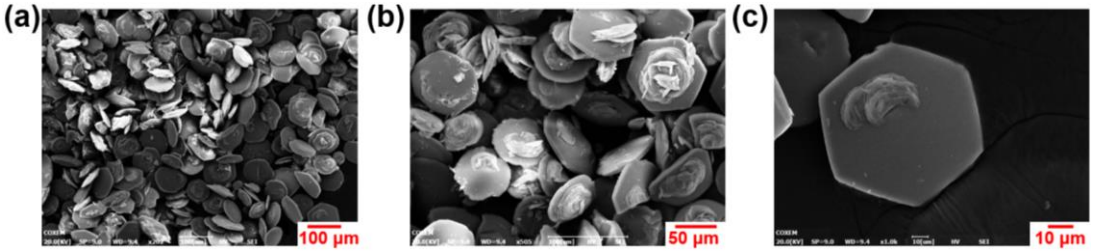

Fig. S36. SEM image of **JNU-206-Gd**.

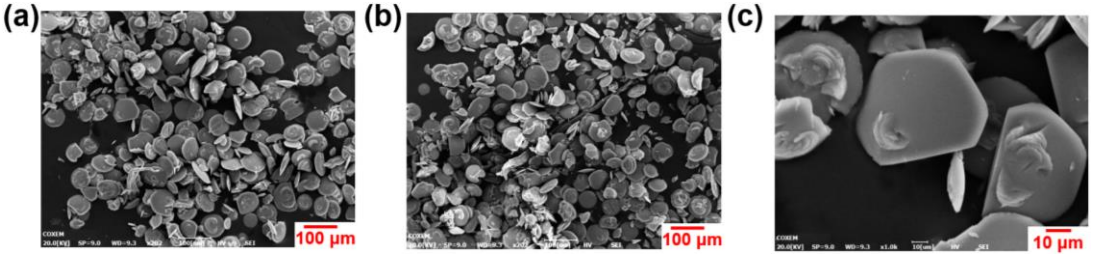

Fig. S37. SEM image of **JNU-206-Tb**.

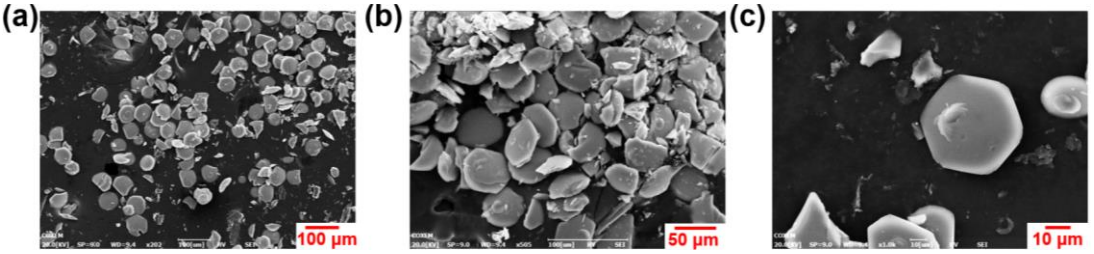

Fig. S38. SEM image of **JNU-206-Dy**.

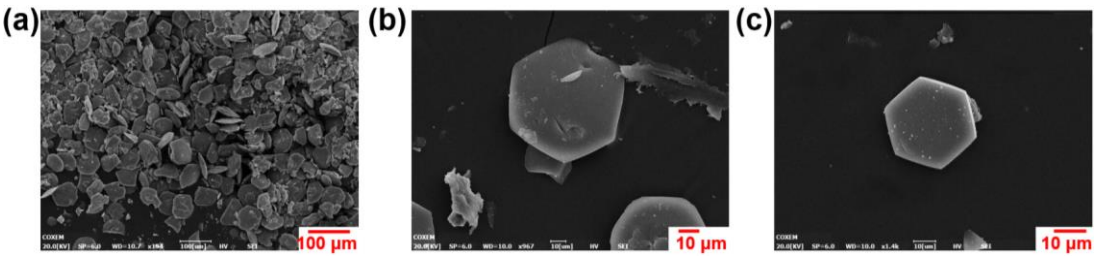

Fig. S39. SEM image of **JNU-206-Ho**.

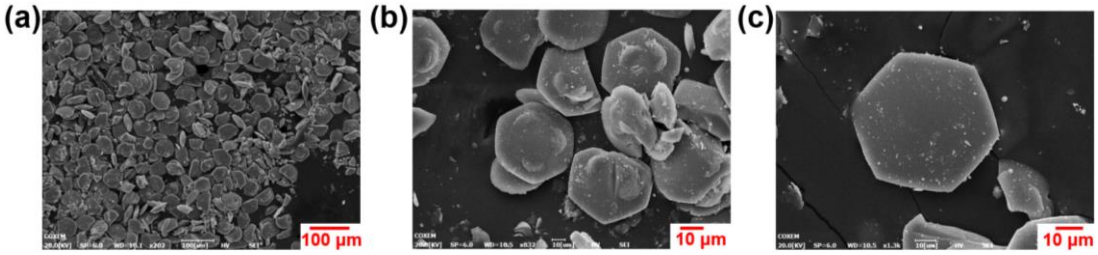

Fig. S40. SEM image of **JNU-206-Er**.

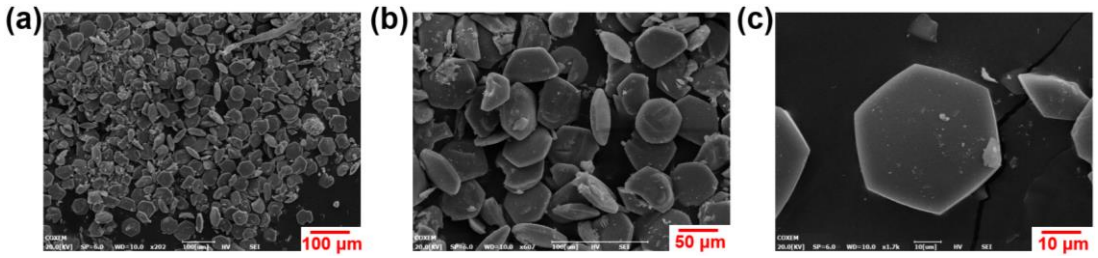

Fig. S41. SEM image of **JNU-206-Tm**.

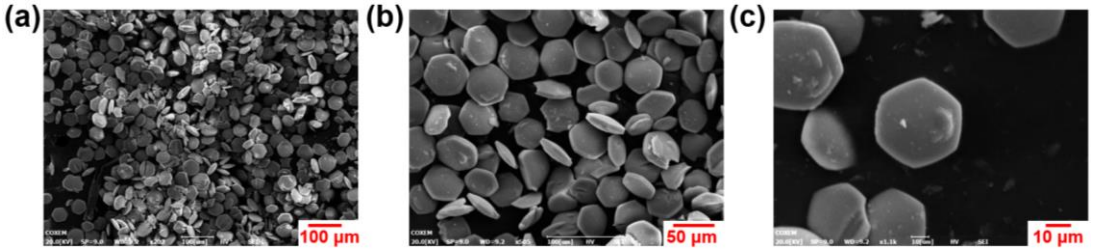

Fig. S42. SEM image of **JNU-206-Yb**.

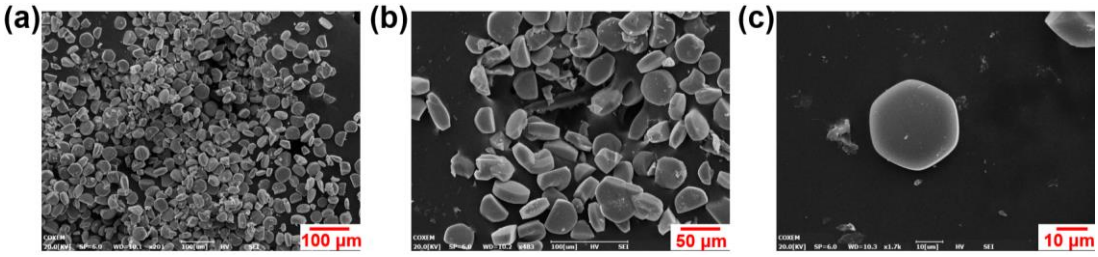

Fig. S43. SEM image of **JNU-206-Lu**.

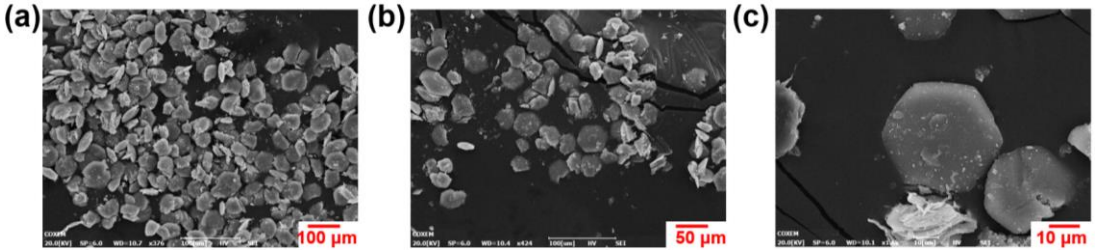

Fig. S44. SEM image of **JNU-206-Y**.

2.5 FT-IR spectra of JNU-206-RE

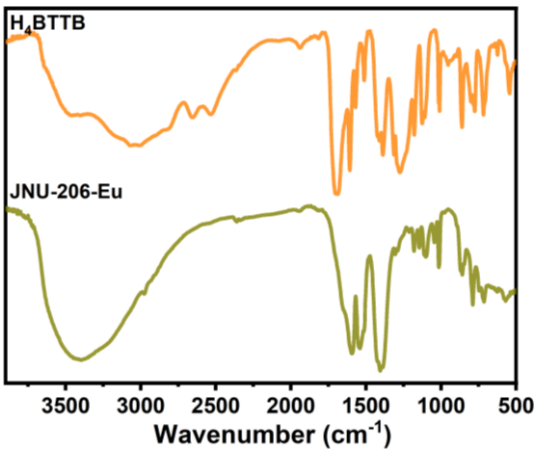

Fig. S45. FT-IR spectra of H_4BTTB and **JNU-206-Eu**.

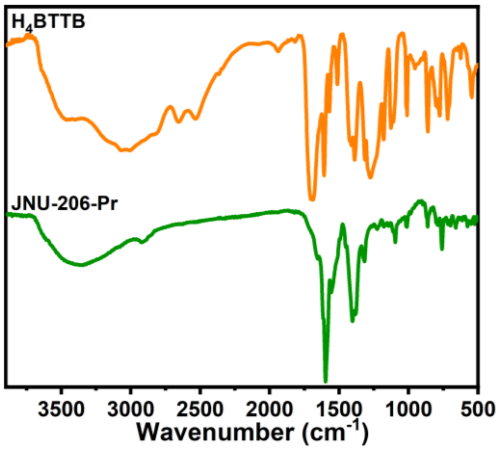

Fig. S46. FT-IR spectra of H_4BTTB and **JNU-206-Pr**.

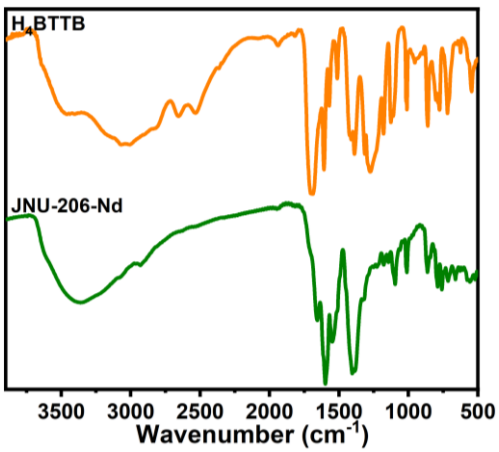

Fig. S47. FT-IR spectra of H_4BTTB and **JNU-206-Nd**.

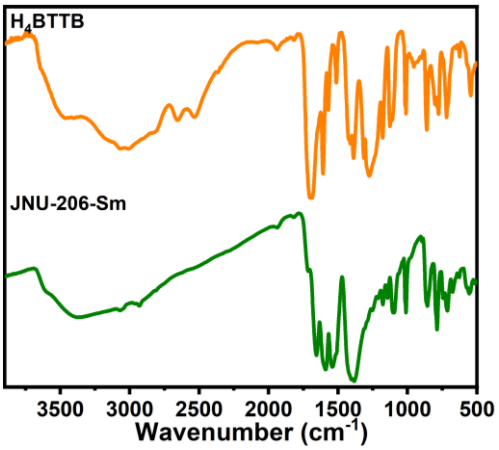

Fig. S48. FT-IR spectra of H_4BTTB and **JNU-206-Sm**.

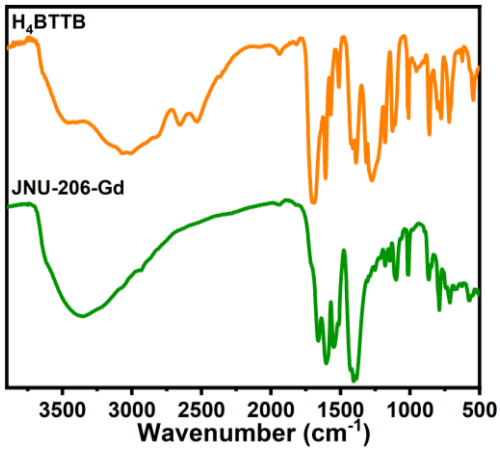

Fig. S49. FT-IR spectra of H_4BTTB and **JNU-206-Gd**.

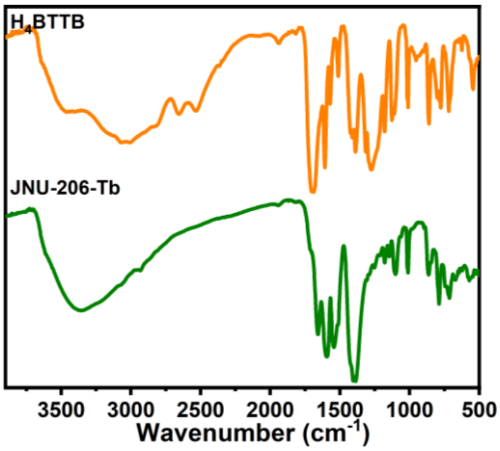

Fig. S50. FT-IR spectra of H_4BTTB and **JNU-206-Tb**.

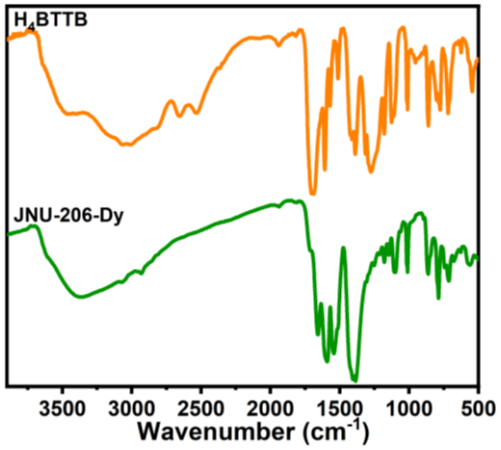

Fig. S51. FT-IR spectra of H_4BTTB and **JNU-206-Dy**.

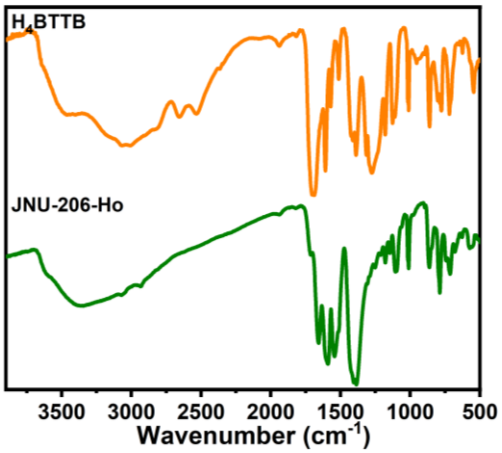

Fig. S52. FT-IR spectra of H_4BTTB and **JNU-206-Ho**.

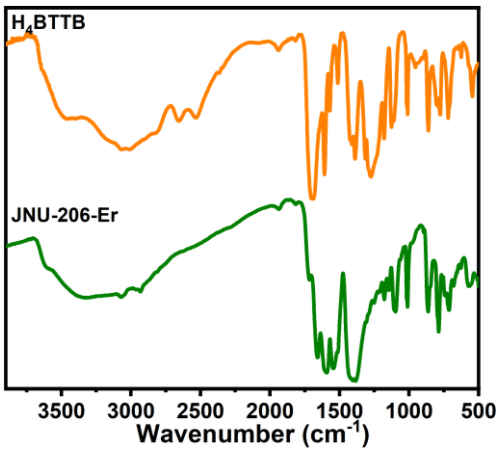

Fig. S53. FT-IR spectra of H_4BTTB and **JNU-206-Er**.

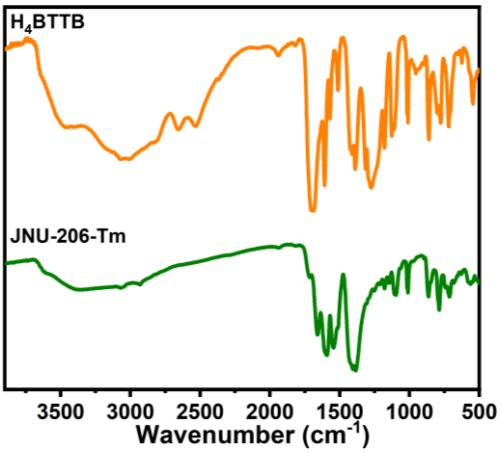

Fig. S54. FT-IR spectra of H_4BTTB and **JNU-206-Tm**.

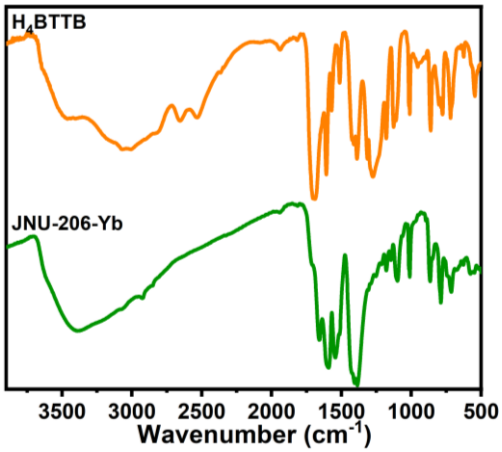

Fig. S55. FT-IR spectra of H_4BTTB and **JNU-206-Yb**.

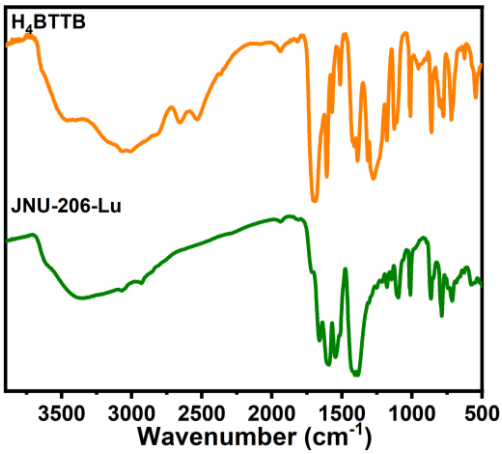

Fig. S56. FT-IR spectra of H_4BTTB and **JNU-206-Lu**.

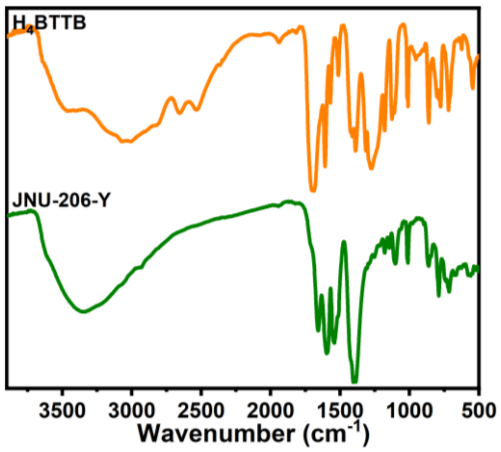

Fig. S57. FT-IR spectra of H_4BTTB and **JNU-206-Y**.

2.6 Crystallographic data of JNU-205-RE

Table S1. Crystal data and structure refinement for **JNU-205-Eu**.

MOF	**JNU-205-Eu**
CCDC number	2142283
Empirical formula	$C_{102}H_{54}Eu_9O_{47}$
Formula weight	3399.09
Crystal system	trigonal
Space group	$P\bar{3}m1$
a/Å	16.5751(3)
b/Å	16.5751(3)
c/Å	12.3843(4)
V/Å^3	5335.01(11)
α/°	90
β/°	90
γ/°	120
Z	1
D_C /g cm^{-3}	1.058
μ /mm^{-1}	18.997
λ /Å	1.54184
T/K	100
Reflections collected	16321
Independent reflections	3887 [*R*int = 0.0429]
Goodness-of-fit on F^2	1.099
R_1[a], wR_2[b] [$I > 2\sigma(I)$]	R_1 = 0.0729, wR_2 = 0.2022
R_1[a], wR_2[b] (all data)	R_1 = 0.0837, wR_2 = 0.2136
Largest diff. peak and hole /e. Å^{-3}	2.40/-2.56

[a] $R_1 = \Sigma||F_o| - |F_c|| / \Sigma|F_o|$

[b] $wR_2 = \{\Sigma[w (F_o^2 - F_c^2)^2]/[w (F_o^2)^2]\}$ 1/2, $[F_o > 4\sigma(F_o)]$

2.7 Crystallographic data of JNU-206-RE

Table S2. Crystal data and structure refinement for **JNU-206-Eu**.

MOF	**JNU-206-Eu**
CCDC number	2142284
Empirical formula	$C_{96}H_{48}Eu_9N_6O_{47}$
Formula weight	3405.04
Crystal system	trigonal
Space group	$P\bar{3}m1$
a/Å	21.9378(6)
b/Å	21.9378(6)
c/Å	12.6523(4)
V/Å^3	5273.3(3)
α/°	90
β/°	90
γ/°	120
Z	1
D_C /g cm^{-3}	1.072
μ /mm^{-1}	19.229
λ /Å	1.54184
T/K	300
Reflections collected	16847
Independent reflections	3913 [*R*int = 0.0653]
Goodness-of-fit on F^2	1.071
R_1[a], wR_2[b] [I > 2σ (I)]	R_1 = 0.0636, wR_2 = 0.1726
R_1[a], wR_2[b] (all data)	R_1 = 0.0737, wR_2 = 0.1828
Largest diff. peak and hole /e. Å^{-3}	1.47/-1.57

[a] $R_1 = \Sigma||F_o| - |F_c|| / \Sigma|F_o|$

[b] $wR_2 = \{\Sigma[w (F_o^2 - F_c^2)^2]/[w (F_o^2)^2]\}$ 1/2, [$F_o > 4\sigma (F_o)$]

Table S3. Crystal data and structure refinement for **JNU-206-Pr**.

MOF	**JNU-206-Pr**
CCDC number	2142285
Empirical formula	$C_{96}H_{48}N_6O_{45.5}Pr_9$
Formula weight	3281.72
Crystal system	hexagonal
Space group	$P6_3/mmc$
a/Å	21.99640(10)
b/Å	21.99640(10)
c/Å	26.1243(2)
V/Å^3	10946.58(13)
α/°	90
β/°	90
γ/°	120
Z	2
D_C /g cm^{-3}	0.996
μ /mm^{-1}	15.426
λ /Å	1.54184
T/K	300
Reflections collected	43387
Independent reflections	4175 [Rint = 0.0479]
Goodness-of-fit on F^2	1.120
R_1[a], wR_2[b] [I > 2σ (I)]	R_1 = *0.0560*, wR_2 = 0.1589
R_1[a], wR_2[b] (all data)	R_1 = 0.0586, wR$_2$ = 0.1631
Largest diff. peak and hole /e. Å^{-3}	3.16/-1.17

[a] $R_1 = \Sigma||F_o| - |F_c|| / \Sigma|F_o|$

[b] $wR_2 = \{\Sigma[w (F_o^2 - F_c^2)^2]/[w (F_o^2)^2]\}$ 1/2, [$F_o > 4\sigma (F_o)$]

Table S4. Crystal data and structure refinement for **JNU-206-Nd**.

MOF	**JNU-206-Nd**
CCDC number	2142286
Empirical formula	$C_{192}H_{96}N_{12}Nd_{18}O_{89}$
Formula weight	6591.12
Crystal system	hexagonal
Space group	$P6_3/mmc$
a/Å	22.0814(2)
b/Å	22.0814(2)
c/Å	25.5403(3)
V/Å^3	10784.7(2)
α/°	90
β/°	90
γ/°	120
Z	1
D_C /g cm^{-3}	1.015
μ /mm^{-1}	16.587
λ /Å	1.54184
T/K	300
Reflections collected	41969
Independent reflections	4120 [Rint = 0.04441]
Goodness-of-fit on F^2	1.059
R_1[a], wR_2[b] [I > 2σ (I)]	R_1 = 0.0953, wR_2 = 0.2348
R_1[a], wR_2[b] (all data)	R_1 = 0.1006, wR_2 = 0.2423
Largest diff. peak and hole /e. Å^{-3}	4.28/-1.16

[a] $R_1 = \Sigma||F_o| - |F_c|| / \Sigma|F_o|$

[b] $wR_2 = \{\Sigma[w (F_o^2 - F_c^2)^2]/[w (F_o^2)^2]\}$ 1/2, $[F_o > 4\sigma (F_o)]$

Table S5. Crystal data and structure refinement for **JNU-206-Sm**.

MOF	**JNU-206-Sm**
CCDC number	2142287
Empirical formula	$C_{96}H_{48}N_6O_{47}Sm_9$
Formula weight	3390.55
Crystal system	trigonal
Space group	$P\bar{3}m1$
a/Å	21.6027(3)
b/Å	21.6027(3)
c/Å	12.4503(2)
V/Å^3	5031.83(16)
α/°	90
β/°	90
γ/°	120
Z	1
D_C /g cm^{-3}	1.119
μ /mm^{-1}	19.794
λ /Å	1.54184
T/K	300
Reflections collected	17949
Independent reflections	3700 [*R*int = 0.0420]
Goodness-of-fit on F^2	1.091
R_1[a], wR_2[b] [I > 2σ (I)]	R_1 = 0.0495, wR_2 = 0.1367
R_1[a], wR_2[b] (all data)	R_1 = 0.0555, wR_2 = 0.1430
Largest diff. peak and hole /e. Å^{-3}	1.82/-1.39

[a] $R_1 = \Sigma||F_o| - |F_c|| / \Sigma|F_o|$

[b] $wR_2 = \{\Sigma[w (F_o^2 - F_c^2)^2]/[w (F_o^2)^2]\}$ 1/2, [$F_o > 4\sigma (F_o)$]

Table S6. Crystal data and structure refinement for **JNU-206-Gd**.

MOF	**JNU-206-Gd**
CCDC number	2142288
Empirical formula	$C_{96}H_{48}Gd_9N_6O_{47}$
Formula weight	3452.65
Crystal system	trigonal
Space group	$P\bar{3}m1$
a/Å	21.8905(17)
b/Å	21.8905(17)
c/Å	12.6457(8)
V/Å^3	5247.9(9)
α/°	90
β/°	90
γ/°	120
Z	1
D_C /g cm^{-3}	1.092
μ /mm^{-1}	18.464
λ /Å	1.54184
T/K	300
Reflections collected	17623
Independent reflections	3882 [*R*int = 0.0614]
Goodness-of-fit on F^2	1.128
R_1[a], wR_2[b] [I > 2σ (I)]	R_1 = 0.0631, wR_2 = 0.1833
R_1[a], wR_2[b] (all data)	R_1 = 0.0709, wR_2 = 0.1946
Largest diff. peak and hole /e. Å^{-3}	1.24/-1.37

[a] $R_1 = \Sigma||F_o| - |F_c|| / \Sigma|F_o|$

[b] $wR_2 = \{\Sigma[w (F_o^2 - F_c^2)^2]/[w (F_o^2)^2]\}$ 1/2, [$F_o > 4\sigma (F_o)$]

Table S7. Crystal data and structure refinement for **JNU-206-Tb**.

MOF	**JNU-206-Tb**
CCDC number	2142289
Empirical formula	$C_{96}H_{48}N_6O_{47}Tb_9$
Formula weight	3467.68
Crystal system	trigonal
Space group	$P\bar{3}m1$
a/Å	21.8367(8)
b/Å	21.8367(8)
c/Å	12.6410(4)
V/Å^3	5220.2(4)
α/°	90
β/°	90
γ/°	120
Z	1
D_C /g cm^{-3}	1.103
μ /mm^{-1}	15.062
λ /Å	1.54184
T/K	300
Reflections collected	278
Independent reflections	3763 [*R*int = 0.0725]
Goodness-of-fit on F^2	1.062
R_1[a], wR_2[b] [I > 2σ (I)]	R_1 = 0.0581, wR_2 = 0.1621
R_1[a], wR_2[b] (all data)	R_1 = 0.0690, wR_2 = 0.1708
Largest diff. peak and hole /e. Å^{-3}	1.62/-1.27

[a] $R_1 = \Sigma||F_o| - |F_c|| / \Sigma|F_o|$

[b] $wR_2 = \{\Sigma[w (F_o^2 - F_c^2)^2]/[w (F_o^2)^2]\}$ 1/2, [$F_o > 4\sigma (F_o)$]

Table S8. Crystal data and structure refinement for **JNU-206-Dy**.

MOF	**JNU-206-Dy**
CCDC number	2142290
Empirical formula	$C_{96}H_{48}Dy_9N_6O_{47}$
Formula weight	3500.04
Crystal system	trigonal
Space group	$P\bar{3}m1$
a/Å	21.7717(2)
b/Å	21.7717(2)
c/Å	12.57240(10)
V/Å^3	5160.99(10)
α/°	90
β/°	90
γ/°	120
Z	1
D_C /g cm^{-3}	1.126
μ /mm^{-1}	17.502
λ /Å	1.54184
T/K	300
Reflections collected	15878
Independent reflections	3878 [*R*int = 0.0289]
Goodness-of-fit on F^2	1.081
R_1[a], wR_2[b] [I > 2σ (I)]	R_1 = 0.0550, wR_2 = 0.1581
R_1[a], wR_2[b] (all data)	R_1 = 0.0586, wR_2 = 0.1621
Largest diff. peak and hole /e. Å^{-3}	1.70/-2.17

[a] $R_1 = \Sigma||F_o| - |F_c|| / \Sigma|F_o|$

[b] $wR_2 = \{\Sigma[w (F_o^2 - F_c^2)^2]/[w (F_o^2)^2]\}$ 1/2, [$F_o > 4\sigma (F_o)$]

Table S9. Crystal data and structure refinement for **JNU-206-Ho**.

MOF	**JNU-206-Ho**
CCDC number	2142291
Empirical formula	$C_{96}H_{42}Ho_9N_6O_{44}$
Formula weight	3467.72
Crystal system	trigonal
Space group	$P\bar{3}m1$
a/Å	22.0118(12)
b/Å	22.0118(12)
c/Å	12.3202(8)
V/Å^3	5169.6(7)
α/°	90
β/°	90
γ/°	120
Z	1
D_C /g cm^{-3}	1.114
μ /mm^{-1}	6.487
λ /Å	1.54184
T/K	300
Reflections collected	16302
Independent reflections	3724 [*R*int = 0.0825]
Goodness-of-fit on F^2	1.067
R_1[a], wR_2[b] [I > 2σ (I)]	R_1 = 0.0558, wR_2 = 0.1543
R_1[a], wR_2[b] (all data)	R_1 = 0.0699, wR_2 = 0.1648
Largest diff. peak and hole /e. Å^{-3}	1.45/-1.14

[a] $R_1 = \Sigma||F_o| - |F_c|| / \Sigma|F_o|$

[b] $wR_2 = \{\Sigma[w (F_o^2 - F_c^2)^2]/[w (F_o^2)^2]\}$ 1/2, [$F_o > 4\sigma (F_o)$]

Table S10. Crystal data and structure refinement for **JNU-206-Er**.

MOF	**JNU-206-Er**
CCDC number	2142292
Empirical formula	$C_{96}H_{48}Er_9N_6O_{47}$
Formula weight	3542.74
Crystal system	trigonal
Space group	$P\bar{3}m1$
a/Å	21.762(3)
b/Å	21.762(3)
c/Å	12.3941(12)
V/Å^3	5083.1(13)
α/°	90
β/°	90
γ/°	120
Z	1
D_C /g cm^{-3}	1.157
μ /mm^{-1}	6.970
λ /Å	1.54184
T/K	300
Reflections collected	15289
Independent reflections	3732 [*R*int = 0.0765]
Goodness-of-fit on F^2	1.095
R_1[a], wR_2[b] [I > 2σ (I)]	R_1 = 0.0729, wR_2 = 0.1992
R_1[a], wR_2[b] (all data)	R_1 = 0.0870, wR_2 = 0.2146
Largest diff. peak and hole /e. Å^{-3}	2.03/-4.08

[a] $R_1 = \Sigma||F_o| - |F_c|| / \Sigma|F_o|$

[b] $wR_2 = \{\Sigma[w (F_o^2 - F_c^2)^2]/[w (F_o^2)^2]\}$ 1/2, [$F_o > 4\sigma (F_o)$]

Table S11. Crystal data and structure refinement for **JNU-206-Tm**.

MOF	**JNU-206-Tm**
CCDC number	2142293
Empirical formula	$C_{96}H_{48}N_6O_{47}Tm_9$
Formula weight	3557.77
Crystal system	trigonal
Space group	$P\bar{3}m1$
a/Å	21.731(2)
b/Å	21.731(2)
c/Å	12.4178(12)
V/Å^3	5078.6(11)
α/°	90
β/°	90
γ/°	120
Z	1
D_C /g cm^{-3}	1.163
μ /mm^{-1}	7.437
λ /Å	1.54184
T/K	300
Reflections collected	12437
Independent reflections	3677 [*R*int = 0.1724]
Goodness-of-fit on F^2	0.114
R_1[a], wR_2[b] [I > 2σ (I)]	R_1 = 0.1202, wR_2 = 0.2777
R_1[a], wR_2[b] (all data)	R_1 = 0.1683, wR_2 = 0.3353
Largest diff. peak and hole /e. Å^{-3}	4.33/-3.17

[a] $R_1 = \Sigma||F_o| - |F_c|| / \Sigma|F_o|$

[b] $wR_2 = \{\Sigma[w (F_o^2 - F_c^2)^2]/[w (F_o^2)^2]\}$ 1/2, [$F_o > 4\sigma (F_o)$]

Table S12. Crystal data and structure refinement for **JNU-206-Yb**.

MOF	**JNU-206-Yb**
CCDC number	2142294
Empirical formula	$C_{96}H_{60}N_6O_{44}Yb_9$
Formula weight	3558.86
Crystal system	trigonal
Space group	$P\bar{3}m1$
a/Å	21.6417(3)
b/Å	21.6417(3)
c/Å	12.4403(2)
V/Å^3	5045.96(16)
α/°	90
β/°	90
γ/°	120
Z	1
D_C /g cm^{-3}	1.171
μ /mm^{-1}	7.770
λ /Å	1.54184
T/K	300
Reflections collected	16044
Independent reflections	3710 [Rint = 0.0426]
Goodness-of-fit on F^2	1.087
R_1[a], wR_2[b] [I > 2σ (I)]	R_1 = 0.0554, wR_2 = 0.1519
R_1[a], wR_2[b] (all data)	R_1 = 0.0610, wR_2 = 0.1578

[a] $R_1 = \Sigma||F_o| - |F_c|| / \Sigma|F_o|$

[b] $wR_2 = \{\Sigma[w (F_o^2 - F_c^2)^2]/[w (F_o^2)^2]\}$ 1/2, [$F_o > 4\sigma (F_o)$]

Table S13. Crystal data and structure refinement for **JNU-206-Lu**.

MOF	**JNU-206-Lu**
CCDC number	2142295
Empirical formula	$C_{96}H_{48}Lu_9N_6O_{47}$
Formula weight	3612.13
Crystal system	trigonal
Space group	$P\bar{3}m1$
a/Å	21.6440(2)
b/Å	21.6440(2)
c/Å	12.41340(10)
V/Å^3	5036.12(10)
α/°	90
β/°	90
γ/°	120
Z	1
D_C /g cm^{-3}	1.191
μ /mm^{-1}	8.518
λ /Å	1.54184
T/K	300
Reflections collected	16865
Independent reflections	3733 [*R*int = 0.0387]
Goodness-of-fit on F^2	1.096
R_1[a], wR_2[b] [$I > 2\sigma(I)$]	R_1 = 0.0413, wR_2 = 0.1144
R_1[a], wR_2[b] (all data)	R_1 = 0.0465, wR_2 = 0.1181
Largest diff. peak and hole /e. Å^{-3}	2.21/-1.75

[a] $R_1 = \Sigma||F_o| - |F_c|| / \Sigma|F_o|$

[b] $wR_2 = \{\Sigma[w (F_o^2 - F_c^2)^2]/[w (F_o^2)^2]\}$ 1/2, $[F_o > 4\sigma(F_o)]$

Table S14. Crystal data and structure refinement for **JNU-206-Y**.

MOF	**JNU-206-Y**
CCDC number	2142296
Empirical formula	$C_{96}H_{48}N_6O_{47}Y_9$
Formula weight	2837.59
Crystal system	trigonal
Space group	$P\bar{3}m1$
a/Å	21.7883(6)
b/Å	21.7883(6)
c/Å	12.4902(4)
V/Å^3	5135.1(3)
α/°	90
β/°	90
γ/°	120
Z	1
D_C /g cm^{-3}	0.918
μ /mm^{-1}	3.674
λ /Å	1.54184
T/K	300
Reflections collected	16976
Independent reflections	3797 [*R*int = 0.0506]
Goodness-of-fit on F^2	1.099
R_1[a], wR_2[b] [I > 2σ (I)]	R_1 = 0.0737, wR_2 = 0.2019
R_1[a], wR_2[b] (all data)	R_1 = 0.0814, wR_2 = 0.2101
Largest diff. peak and hole /e. Å^{-3}	2.62/-1.95

[a] $R_1 = \Sigma||F_o| - |F_c|| / \Sigma|F_o|$

[b] $wR_2 = \{\Sigma[w (F_o^2 - F_c^2)^2]/[w (F_o^2)^2]\}$ 1/2, [$F_o > 4\sigma (F_o)$]

2.8 TGA of JNU-205-RE and JNU-206-RE

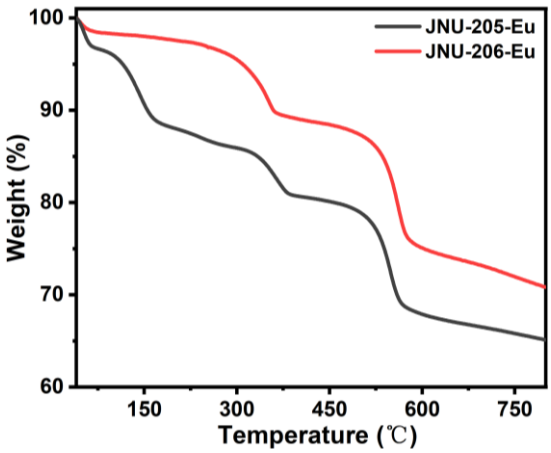

Fig. S58. TGA of **JNU-205-Eu** and **JNU-206-Eu**.

2.9 PXRD patterns of JNU-205-RE and JNU-206-RE

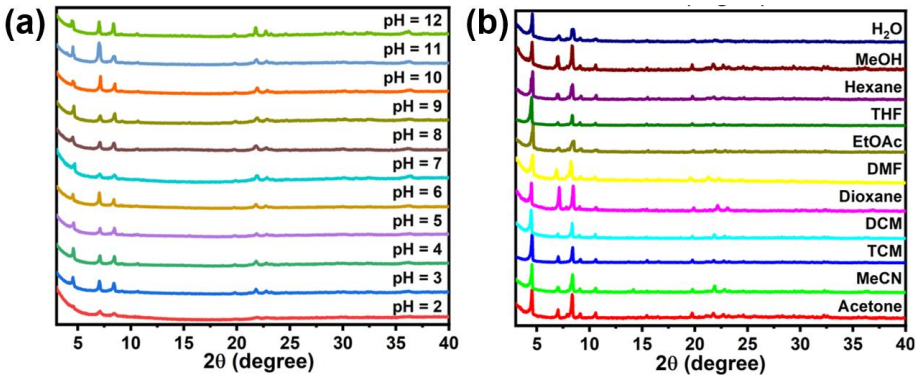

Fig. S59. Comparison of the PXRD patterns of **JNU-205-Eu** after being treated with (a) aqueous solutions at different pH values and (b) different organic solvents.

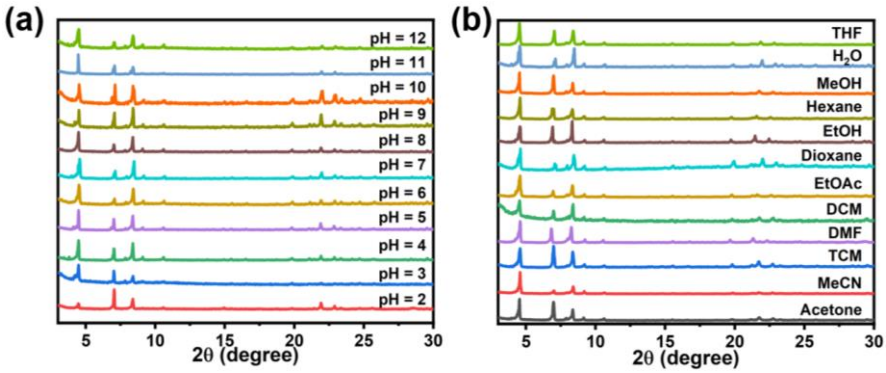

Fig. S60. Comparison of the PXRD patterns of **JNU-206-Eu** after being treated with (a) aqueous solutions at different pH values and (b) different organic solvents.

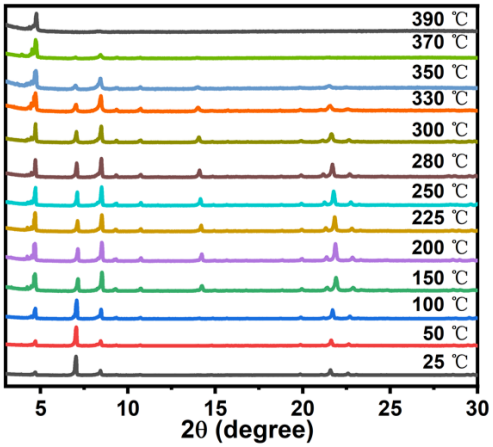

Fig. S61. *In-situ* variable-temperature PXRD (VT-PXRD) of **JNU-206-Eu**.

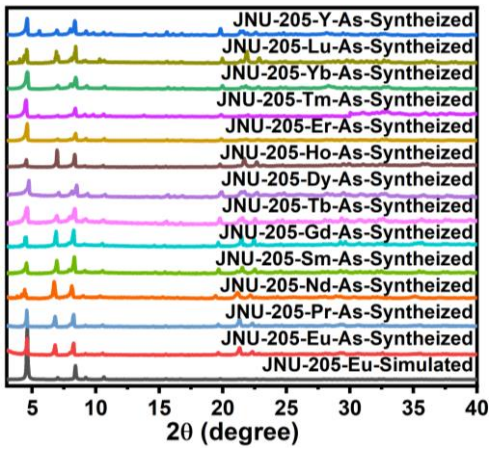

Fig. S62. PXRD patterns of **JNU-205-RE**.

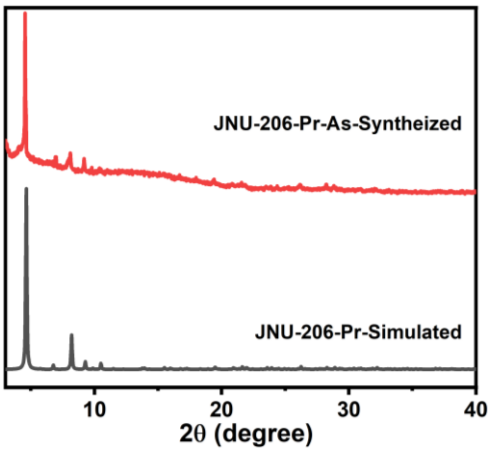

Fig. S63. PXRD patterns of **JNU-206-Pr**.

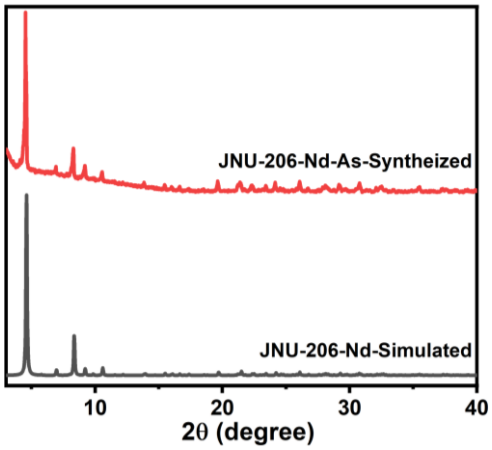

Fig. S64. PXRD patterns of **JNU-206-Nd**.

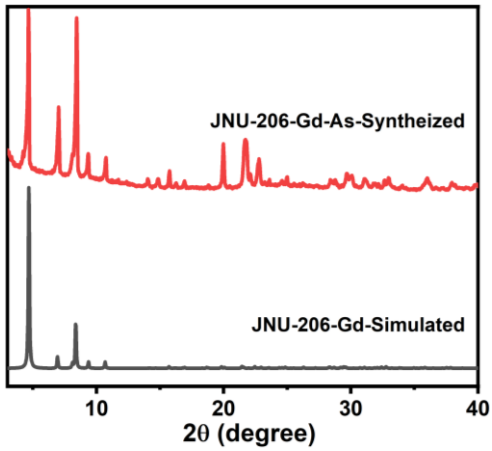

Fig. S65. PXRD patterns of **JNU-206-Gd**.

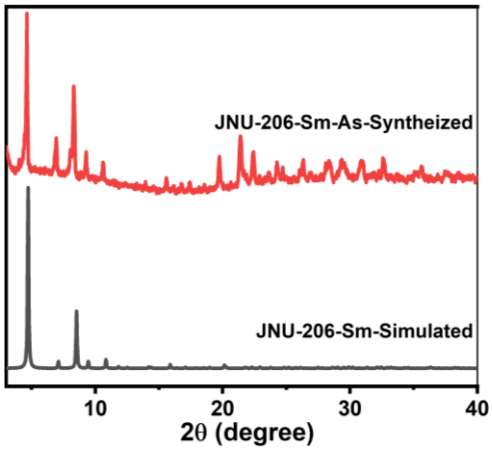

Fig. S66. PXRD patterns of **JNU-206-Sm**.

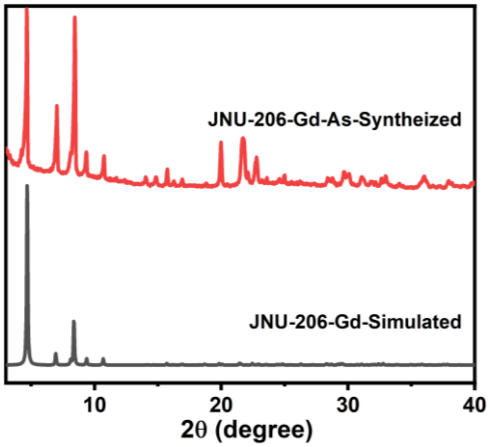

Fig. S67. PXRD patterns of **JNU-206-Gd**.

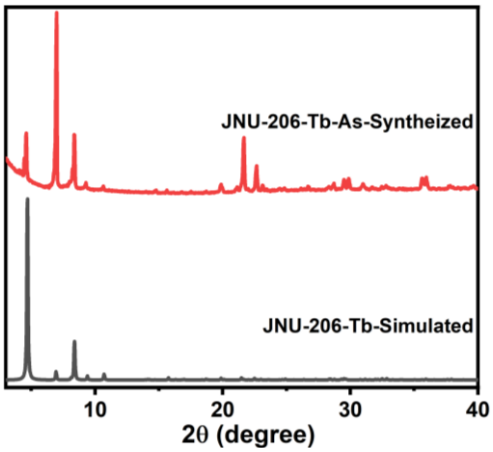

Fig. S68. PXRD patterns of **JNU-206-Tb**.

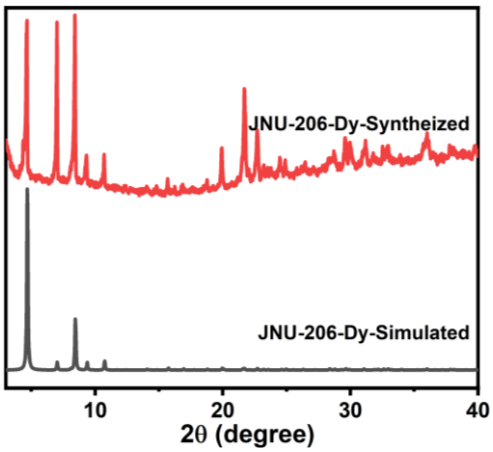

Fig. S69. PXRD patterns of **JNU-206-Dy**.

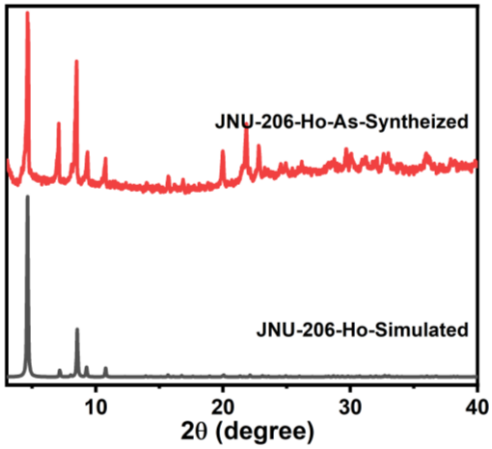

Fig. S70. PXRD patterns of **JNU-206-Ho**.

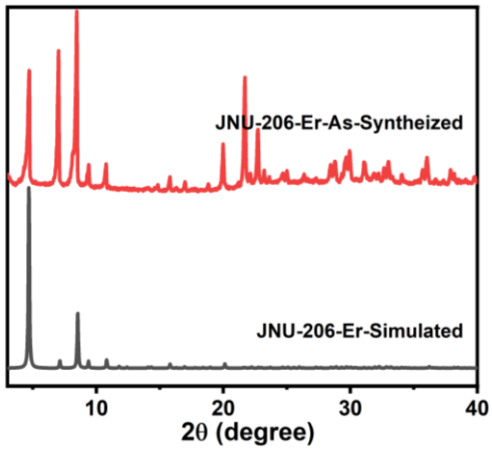

Fig. S71. PXRD patterns of **JNU-206-Er**.

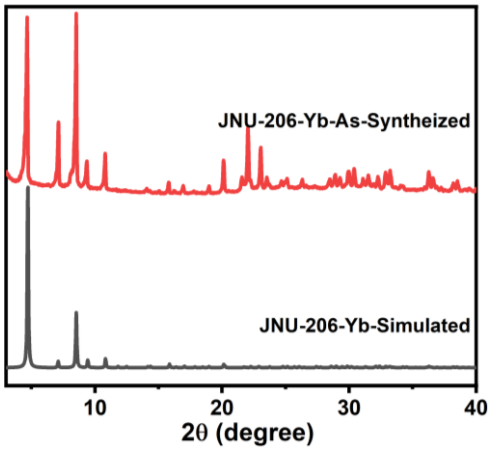

Fig. S72. PXRD patterns of **JNU-206-Yb**.

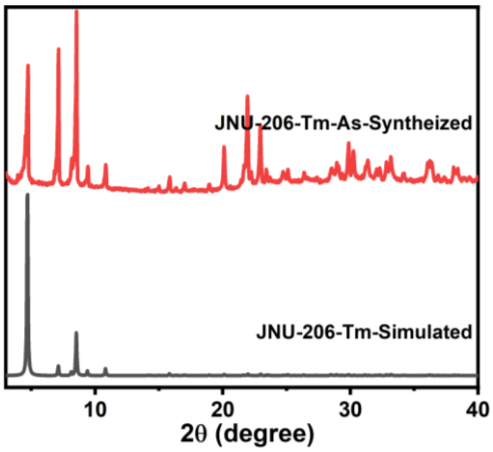

Fig. S73. PXRD patterns of **JNU-206-Tm**.

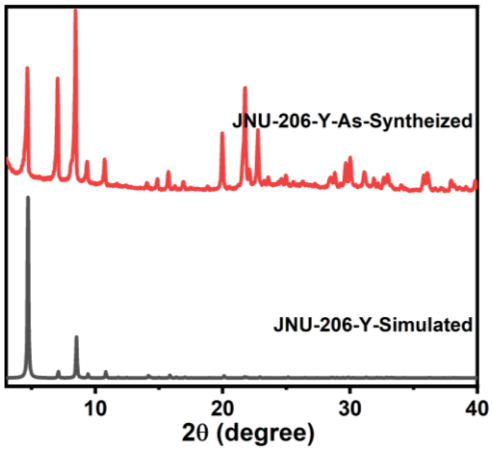

Fig. S74. PXRD patterns of **JNU-206-Y**.

2.10 Luminescence spectra of JNU-205-RE and JNU-206-RE

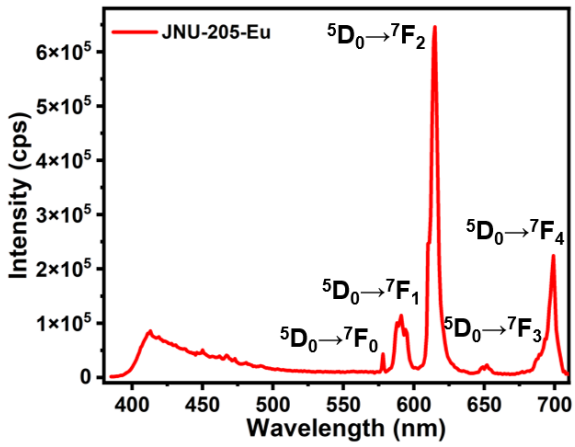

Fig. S75. Luminescence emission spectra (λ_{ex} = 365 nm, slit = 2 nm) of **JNU-205-Eu**.

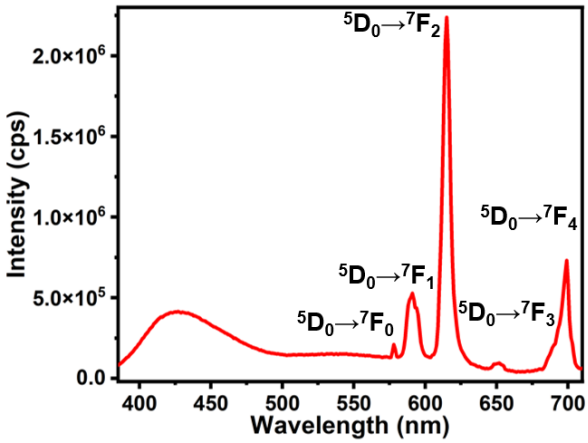

Fig. S76. Luminescence emission spectra (λ_{ex} = 365 nm) of **JNU-206-Eu** in aqueous suspensions.

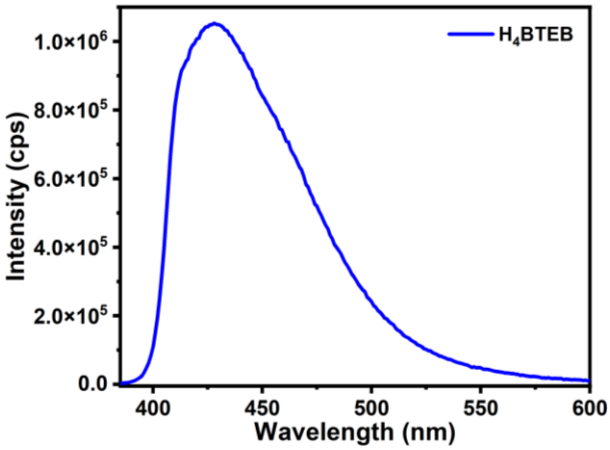

Fig. S77. Luminescence emission spectrum of H_4BTEB.

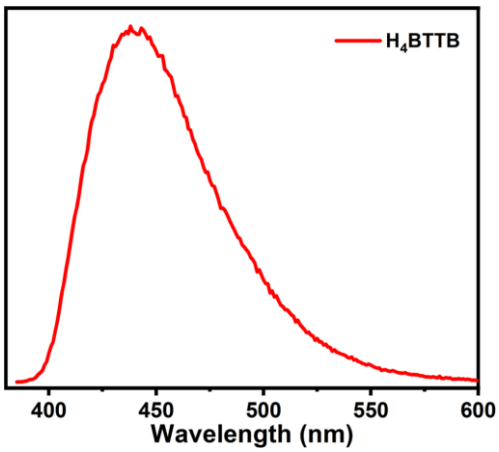

Fig. S78. Luminescence emission spectrum of H_4BTTB.

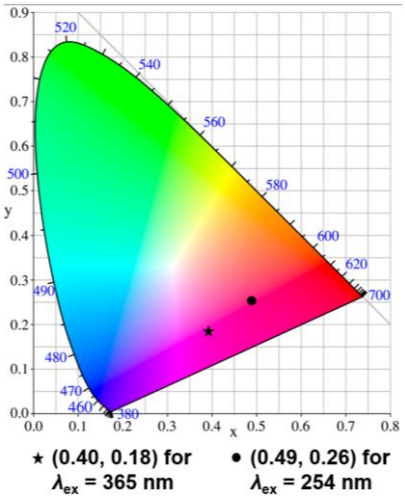

Fig. S79. CIE chromaticity diagram of **JNU-206-Eu** in solid state by varying excitation energy (at room temperature).

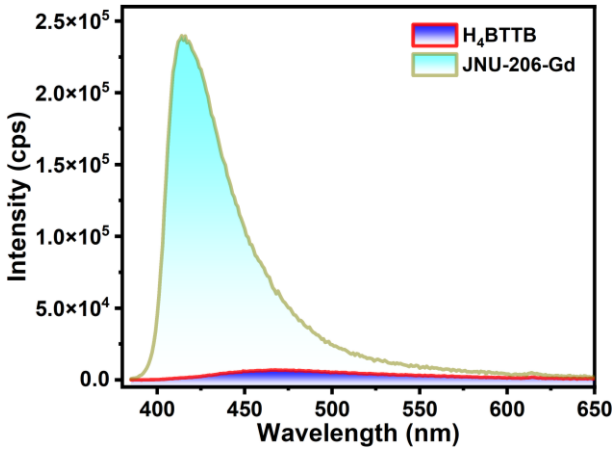

Fig. S80. Luminescence emission spectra of H_4BTTB and **JNU-206-Gd** (λ_{ex} = 365 nm, slit = 0.5).

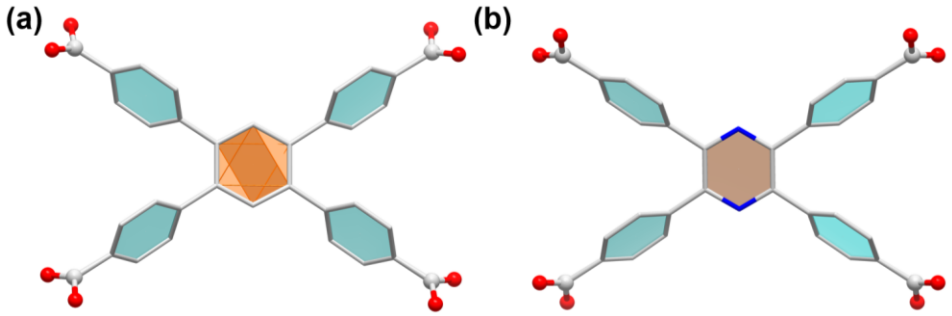

Fig. S81. Linker distortion between the phenyl plane and the pyrazinyl/phenyl plane (a) BTEB and (b) BTTB.

Section 3. Luminescence sensing of tetracyclines

Luminescence studies were carried out by using aqueous suspensions of **JNU-206-Eu** at room temperature. Ground **JNU-206-Eu** (30 mg) was subjected to dispersion in deionized water (100 mL) and ultrasonication for half hour before uses. To 2.7 mL of the above-prepared **JNU-206-Eu** suspension, add 0.3 mL of aqueous solutions of TC, CTC, and OTC at different concentrations Their uminescence emissions were monitored.

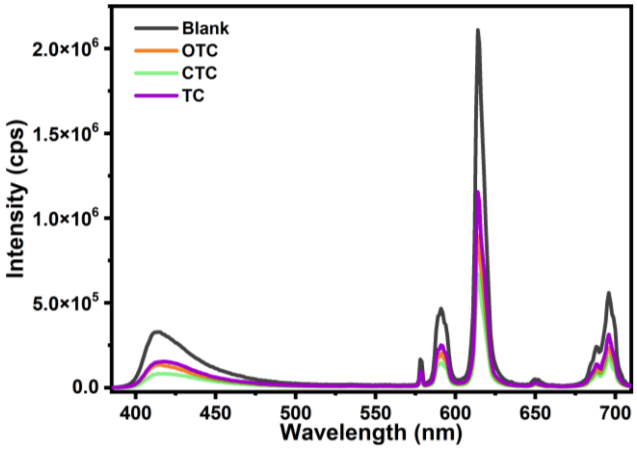

Fig. S82. Luminescent emission spectra of **JNU-206-Eu** suspensions in the presence of 0.5 mM of different antibiotics under excitation of 365 nm.

Table S15. Comparison of detection capacities of selected porous materials for tetracyclines (TCs).

MOF Materials	TCs	linear range (μM)	Quenching constant (M^{-1})	LOD (μM)	Solvent	Recyclability	Ref
In-sbdc	TC OTC CTC	0–30	NA	0.28 0.30 0.30	Bis-Tris-HCl buffer (10 mM, pH = 6.0)	Yes	4
PCN-128Y	TC	0–1	9.84×10^5	0.03	water	NA	5
$([Tb(HL)L(H2O)]_n$	OTC TC	0–50 0–50	2.18×10^4 1.39×10^4	0.02 0.03	water	NA	6
Tb-MOF	TC	100–244	6.75×10^3	0.18	water	Yes	7
Al-MOF@Mo/Zn-MOF	DOX	0.001–46.67	3.32×10^4	0.56 nM	water	Yes	8

	TC	0.001–53.33	3.51×10^4	0.53 nM			
	OTC		3.22×10^4	0.58 nM			
	CTC		2.19×10^4	0.86 nM			
Eu-MOF	TC	0–140	$7,89 \times 10^3$	0.04	water	NA	9
RhB@ZIF-8	TC	0–46	8.6×10^4	0.11	water	Yes	10
	OTC		7.6×10^4	0.14			
FSS@ZIF-8	TC		4.6×10^4	0.17			
	OTC		5.5×10^4	0.16			
NH_2-MIL-53(Al)	TC	0−73	4.6×10^4	0.02	PBS (pH = 8.0, 0.01 M)	NA	11
	DOX	0−66.67	2.9×10^4	0.04			
	OTC	0−86	1.9×10^4	0.06			
ZIF-8/NH_2-MIL-53(Al)	DOX	0.004−25.7mg/L	NA	1.2μg/L	water	Yes	12
	TC	0.004−38.5mg/L					
	OTC	0.004-32.1mg/L					
	CTC	0.005-25.7 mg/L		2.2μg/L			
$Eu_2(BIPA)_3(H_2O)$	TC	0.05−60	8.77×10^5	3 nM	aqueous solution (pH 9)	NA	13
FSS@MOF-5/GMP-Eu	TC	0−20	1.08×10^5	0.02	DMF-water solution, 5/5, v/v	NA	14
Eu-CBO@ZIF-8	TC	0−70	NA	0.02	water	NA	15
{[Cd(2-F-tzba)(H_2O)]·1.5H_2O}$_n$	DOX	0−33.23	2.81×10^4	11.76	water	Yes	16
	TC		3.51×10^4	8.97			
	OTC		2.44×10^4	13.53			
	CTC		1.79×10^4	18.39			
{[Cd(3-F-tzba)(H_2O)]·1.5H_2O}$_n$	DOX	0−33.23	2.66×10^4	12.40	water	Yes	
	TC		3.51×10^4	9.39			
	OTC		2.32×10^4	14.25			
	CTC		1.71×10^4	19.29			
ZIF-8-on-Tb-dpn	TC	0−10	6.55×10^5	5.6 nM	water	Yes	17
Zn-BTEC	CTC	0−8	6.18×10^6	0.03	Tris-HCl buffer solution (pH = 8)	NA	18
JNU-205-Eu	OTC	0−50	7.68×10^3	1.07	water	Yes	**This work**
JNU-206-Eu	TC	0−80	1.33×10^4	0.62	water	Yes	**This**

OTC	0−50	2.37×10^4	0.35	work
CTC	0−80	2.3×10^4	0.36	

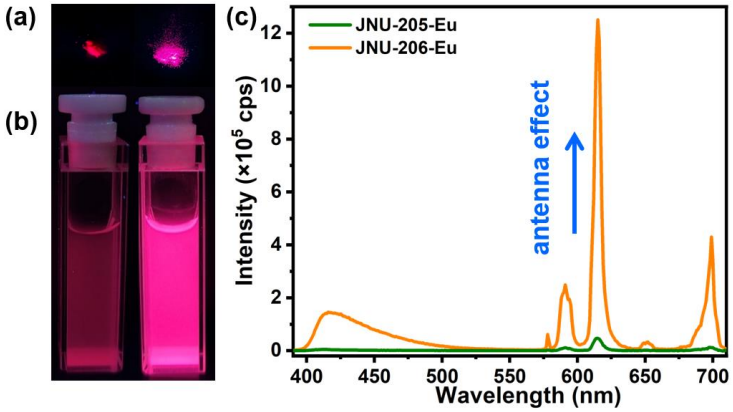

Fig. S83. Photographs of (a) Solid-state and (b) suspension-state **JNU-205-Eu** (left) and **JNU-206-Eu** (right) under hand-held 365 nm UV lamp. (c) Suspension-state emission spectra of **JNU-205-Eu** and **JNU-206-Eu** (30 mg/100 mL, λ_{ex} = 365 nm, slit = 1nm).

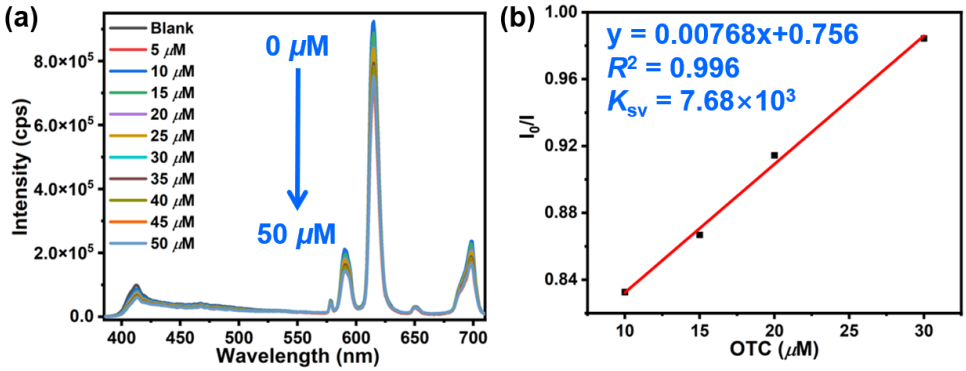

Fig. S84. (a) Luminescence titration of aqueous suspension of **JNU-205-Eu** with aqueous solution of OTC as titrant (0−50 μM) (b) S−V plot of I_0/I versus OTC concentration (λ_{ex} = 365 nm, 10−30 μM).

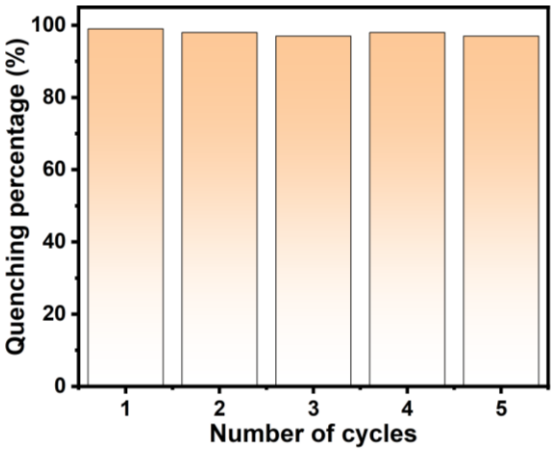

Fig. S85. Quenching efficiency of **JNU-206-Eu** in five cycles of sensing experiments.

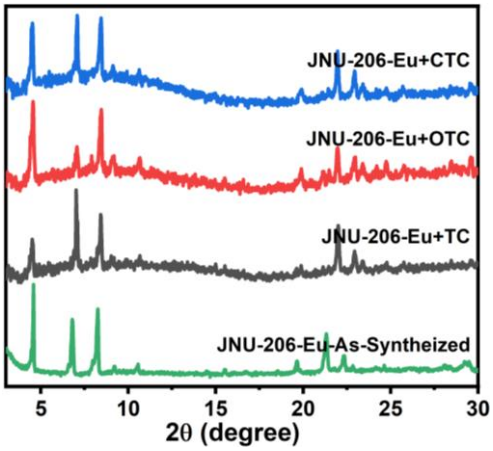

Fig. S86. PXRD patterns of **JNU-206-Eu** before and after being soaking in different aqueous solutions of antibiotics.

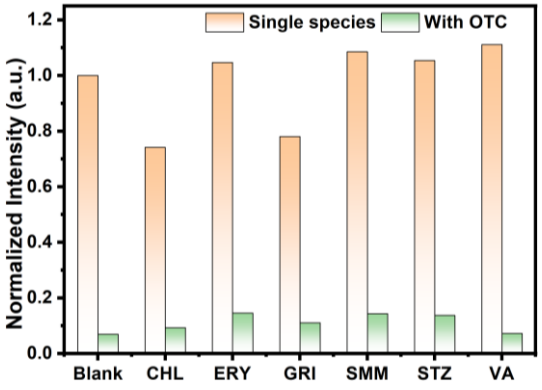

Fig. S87. Comparison of luminescence emission intensity (at 615 nm) of **JNU-206-Eu** upon addition of interfering antibiotics and then OTC.

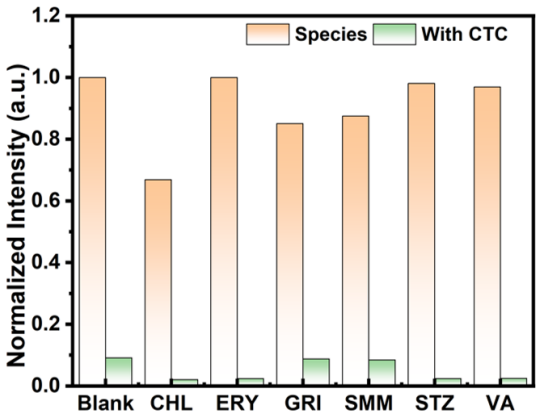

Fig. S88. Comparison of luminescence emission intensity (at 615 nm) of **JNU-206-Eu** upon addition of interfering antibiotics and then CTC.

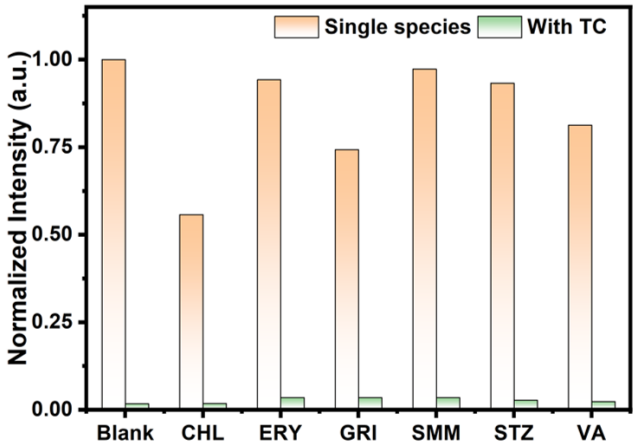

Fig. S89. Comparison of luminescence emission intensity (at 615 nm) of **JNU-206-Eu** upon addition of interfering antibiotics and then TC.

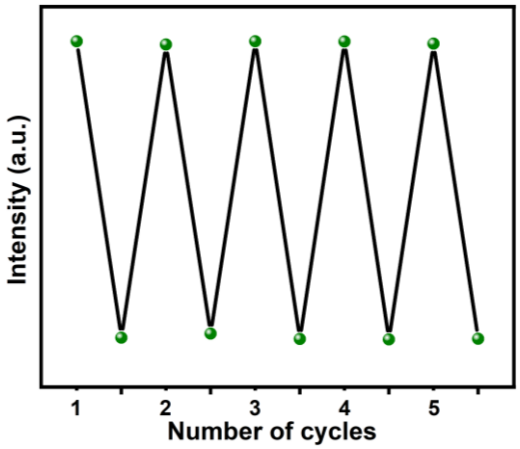

Fig. S90. Five cycles of sensing experiments of **JNU-206-Eu** for OTC in the presence of interfering antibiotics.

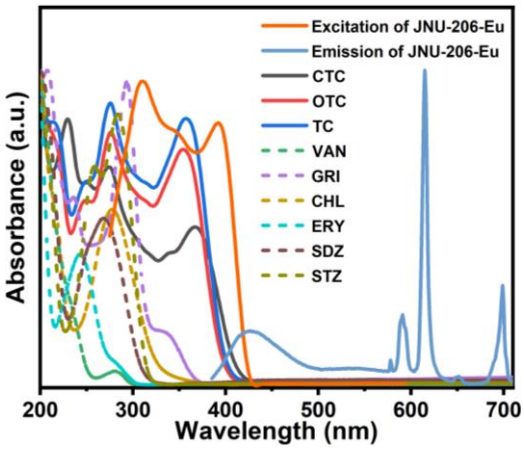

Fig. S91. UV–visible absorption spectra of antibiotics, and excitation and emission spectra of **JNU-206-Eu**.

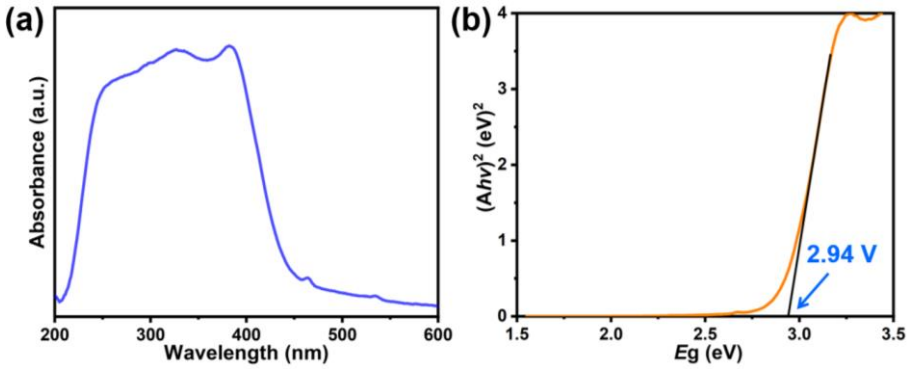

Fig. S92. (a) UV−visible diffuse reflectance spectrum of **JNU-206-Eu;** (b) Tauc plot for **JNU-206-Eu**.

Section 4. Electrochemical measurements and computational details

4.1. Electrochemical measurements

Cyclic voltammetry (CV) measurements were performed on a CHI 660E electrochemical workstation with a three-electrode cell in the supporting electrolyte. The supporting electrolyte consists of a 0.1 M solution of tetrabutylammonium hexafluorophosphate ($TBAPF_6$) in acetonitrile at a scan rate of 50 mV s^{-1} at room temperature. Platinum plate was used as the working electrode, with $Ag/AgNO_3$ (0.1 M $AgNO_3$ in acetonitrile) as the reference electrode and platinum wire as the counter

electrode. The sample preparation method is as follows: 4 mg of sample powder was uniformly dispersed in 1 mL of methanol solution containing 100 μL of 5 wt % Nafion, and the mixture was dropped on the surface of the Platinum plate electrode and dried in a oven. The $Ag/AgNO_3$ reference electrode was calibrated using a ferrocene/ferrocenium redox couple as an external standard, whose oxidation potential is set at -4.80 eV with respect to zero vacuum level. Under this condition, the onset oxidation potential of ferrocene was −0.05 V versus Ag/Ag^+. The LUMO level was calculated according to the first reduction potential based on the equation $E_{LUMO} = -(\varphi^{red} + 4.82)$ (eV).

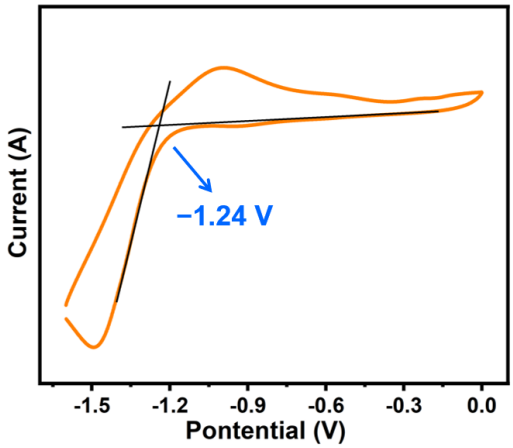

Fig. S93. CV curve of **JNU-206-Eu** in CH_3CN

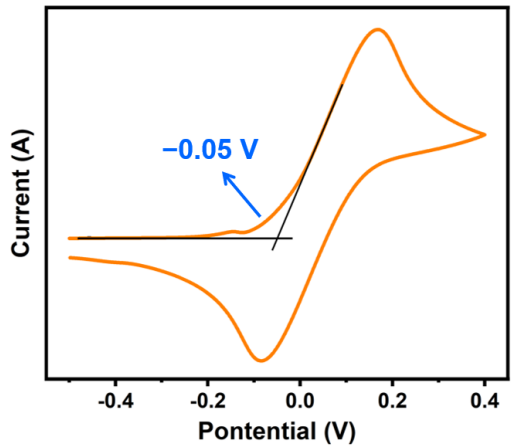

Fig. S94. CV curve of ferrocene in CH_3CN.

4.2. Computational details

The CTC, TC, and CTC molecules were fully optimized by density functional theory (DFT) employing B3LYP functional[19] with def2-tzvp basis set[20] for all atoms. All calculations were performed within Gaussian 09 program[21].

4.3. Lifetime Decay of JNU-206-Eu

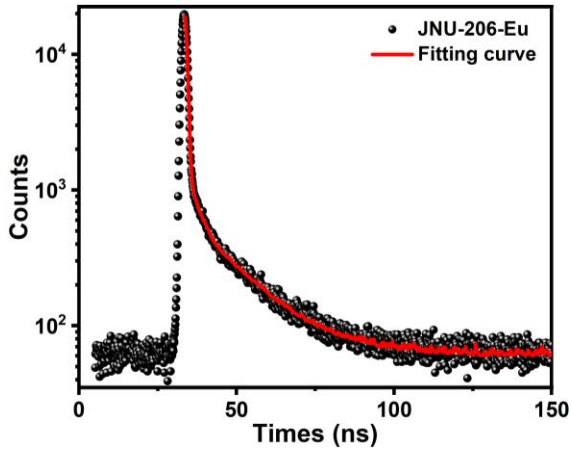

Fig. S95. Time-resolved fluorescence decay spectrum of **JNU-206-Eu**.

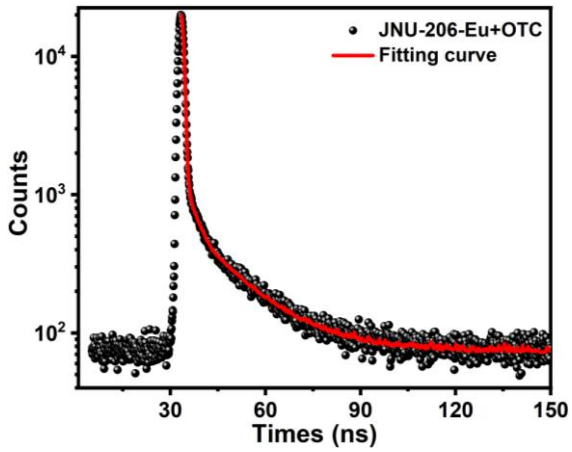

Fig. S96. Time-resolved fluorescence decay spectrum of **JNU-206-Eu+OTC**.

Table S16. Fitting data of the photoluminescence decay of **JNU-206-Eu** and **JNU-206-Eu+OTC**.

	A1	A2	A3	τ_1	τ_2	τ_3	τ_{av} (ns)	Chi2

JNU-206-Eu	4.67659E-03	1.629046E-03	0.500968	1.828024E-09	1.560675E-08	2.507635E-10	0.31	1.12618
JNU-206-Eu+OTC	4.81822E-03	1.718022E-03	0.487217	1.811645E-09	1.536926E-08	2.509547E-10	0.31	1.08757

$\tau_{av} = (A1\times\tau_1^2+A2\times\tau_2^2+A3\times\tau_3^2)/(A1\times\tau_1+A2\times\tau_2+A3\times\tau_3)$.

4.4. XPS of JNU-206-Eu

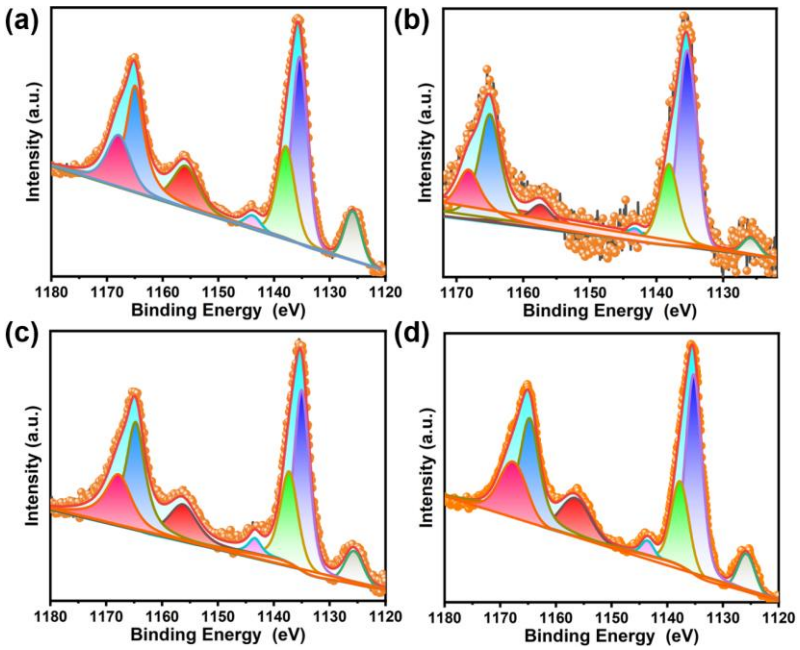

Fig. S97. Eu 3d XPS spectra of (a) **JNU-206-Eu**, (b) **JNU-206-Eu-OTC,** (c) **JNU-206-Eu-TC** and (d) **JNU-206-Eu-CTC**.

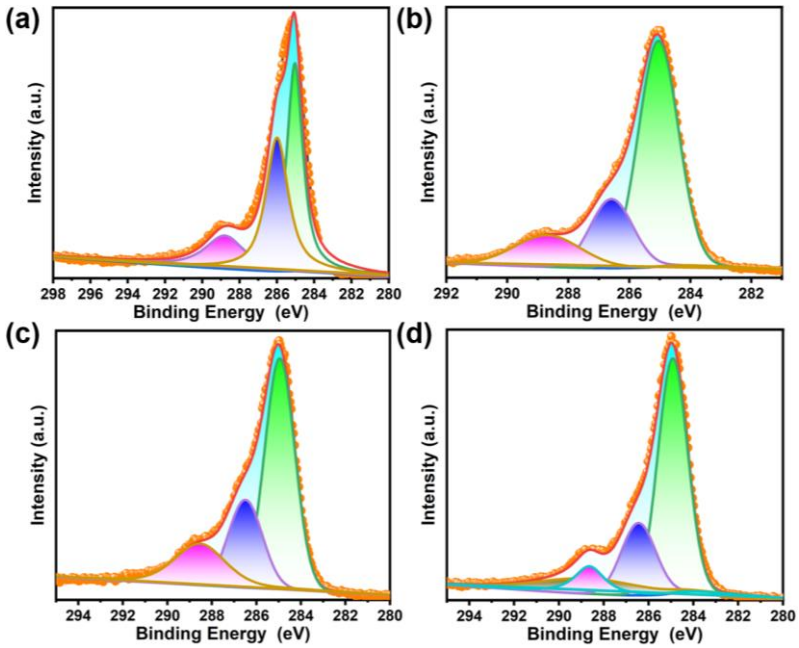

Fig. S98. C 1s XPS spectra of (a) **JNU-206-Eu**, (b) **JNU-206-Eu-OTC,** (c) **JNU-206-Eu-TC** and (d) **JNU-206-Eu-CTC**.

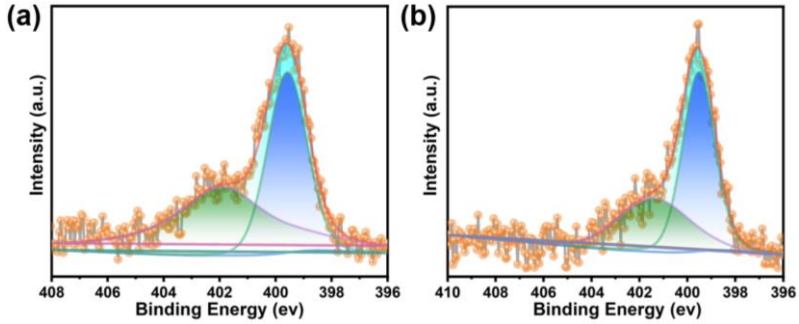

Fig. S99. N 1s XPS spectra of (a) **JNU-206-Eu-TC** and (d) **JNU-206-Eu-CTC**.

Table S17. XPS data for **JNU-206-Eu**, **JNU-206-Eu-OTC**, **JNU-206-Eu-TC**, and **JNU-206-Eu-CTC**.

	JNU-206-Eu	**JNU-206-Eu-OTC**	**JNU-206-Eu-TC**	**JNU-206-Eu-CTC**
Eu	1125.85, 1135.39	1125.88, 1135.38	1125.64, 1135.00	1125.80, 1135.25
	1137.90, 1143.80	1138.15, 1143.27	1137.26, 1143.38	1137.72, 1143.56
	1155.88, 1164.96	1157.39, 1165.02	1156.22, 1164.73	1156.45, 1164.73
	1167.90	1168.21	1167.77	1167.65
C	285.04, 285.99	285.05, 286.58	284.95, 286.50	284.92, 286.45
	288.80	288.68	288.54	288.69, 288.64
N	399.58, 400.87	399.84, 402.20	399.56, 401.91	399.53, 401.39

4.5. Fabrication of JNU-206-Eu-PCL strip

0.15 g of polycaprolactone (PCL, Mr ≈ 80000) was dissolved in 2 mL of dichloromethane. then, 15 mg of ground **JNU-206-Eu** was added to the solution. The mixture was stirred for 30 min to obtain well-dispersed solution, and the homogeneous solution was dropped onto the glass substrate at room temperature. The flexible membrane was obtained, washed with water, and air-dried.

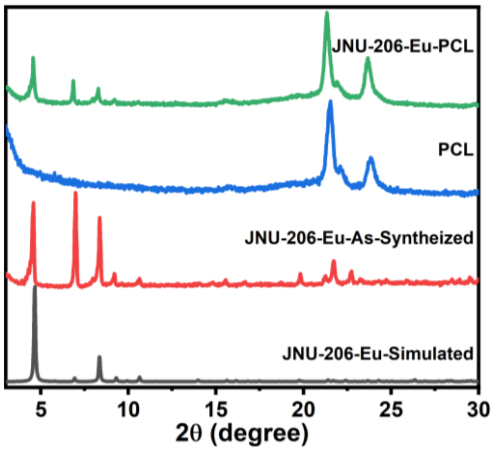

Fig. S100. PXRD patterns of **JNU-206-Eu-PCL**.

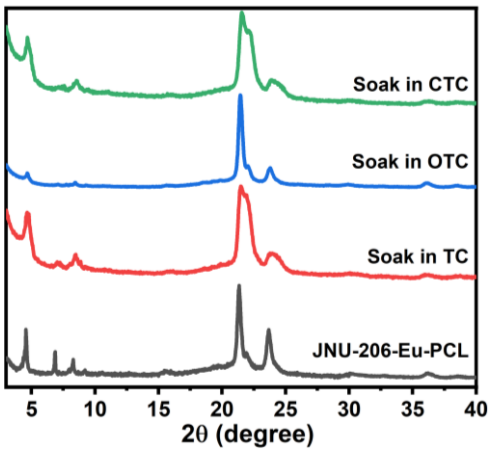

Fig. S101. PXRD patterns of **JNU-206-Eu-PCL** before and after being soaked in different aqueous solutions of antibiotics.

Appendix

^{1}H and ^{13}C NMR spectra for organic intermediates and linkers.

^{1}H NMR (400 MHz, CD_2Cl_2) spectrum of intermediate C.

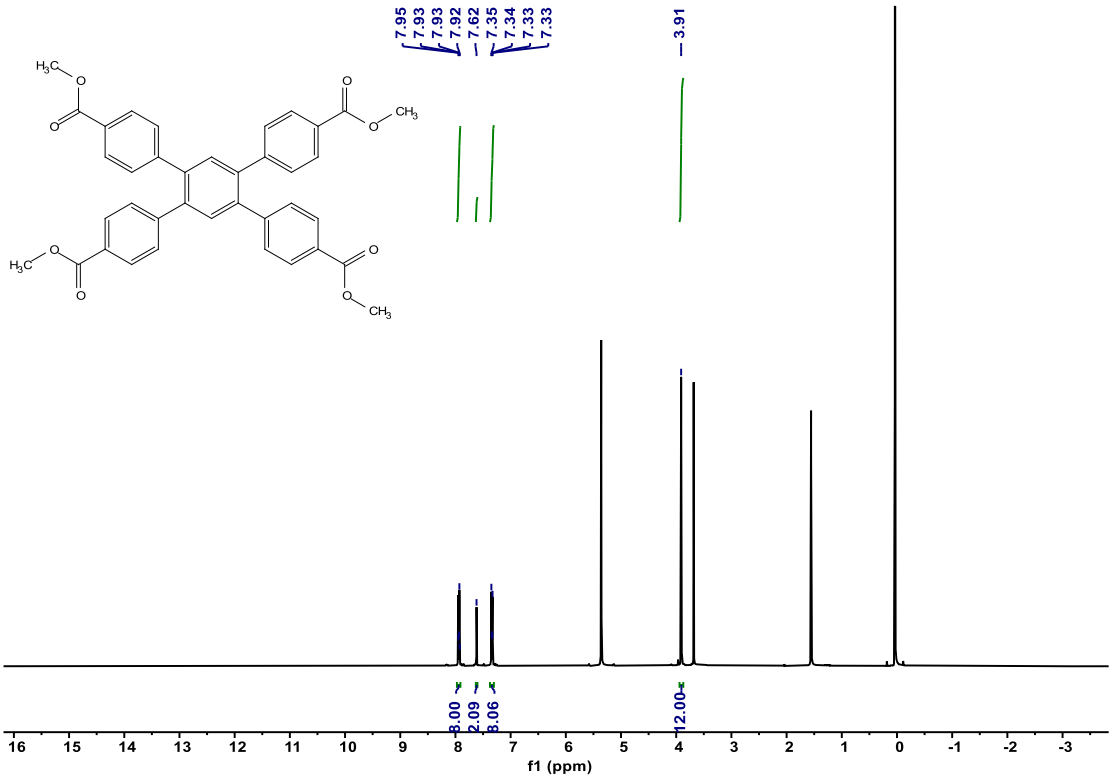

^{13}C NMR (100 MHz, CD_2Cl_2) spectrum of intermediate C.

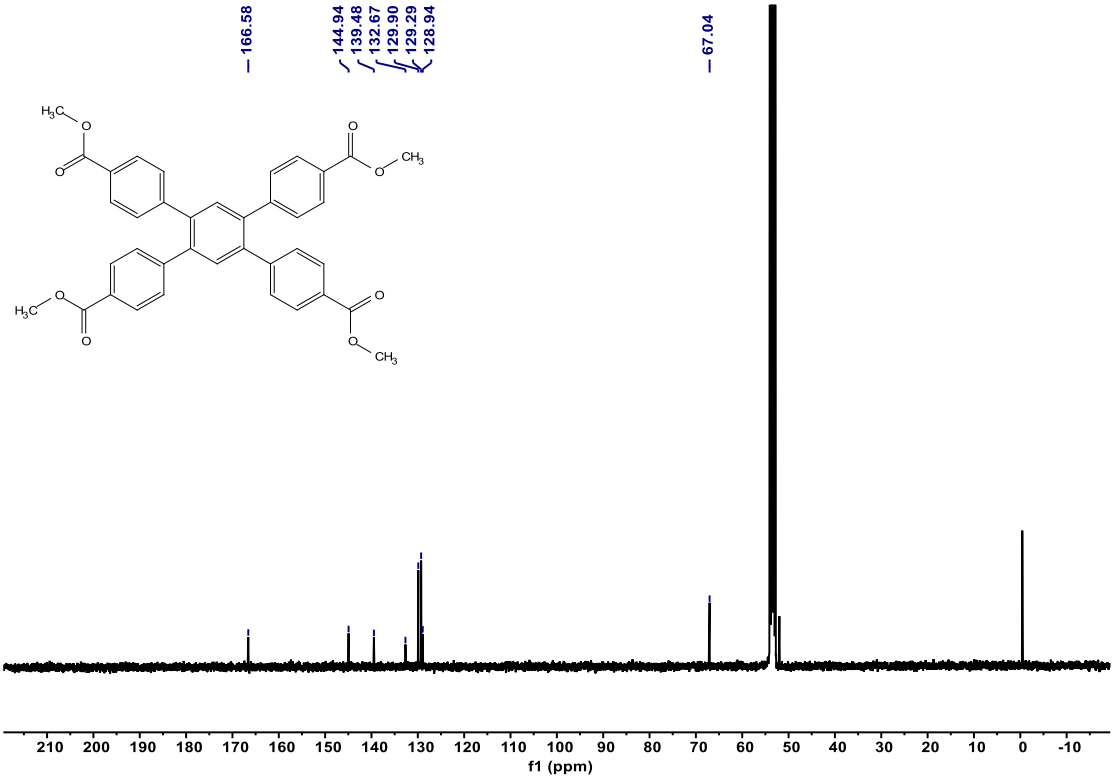

^{1}H NMR (400 MHz, DMSO) spectrum of H_4BTEB.

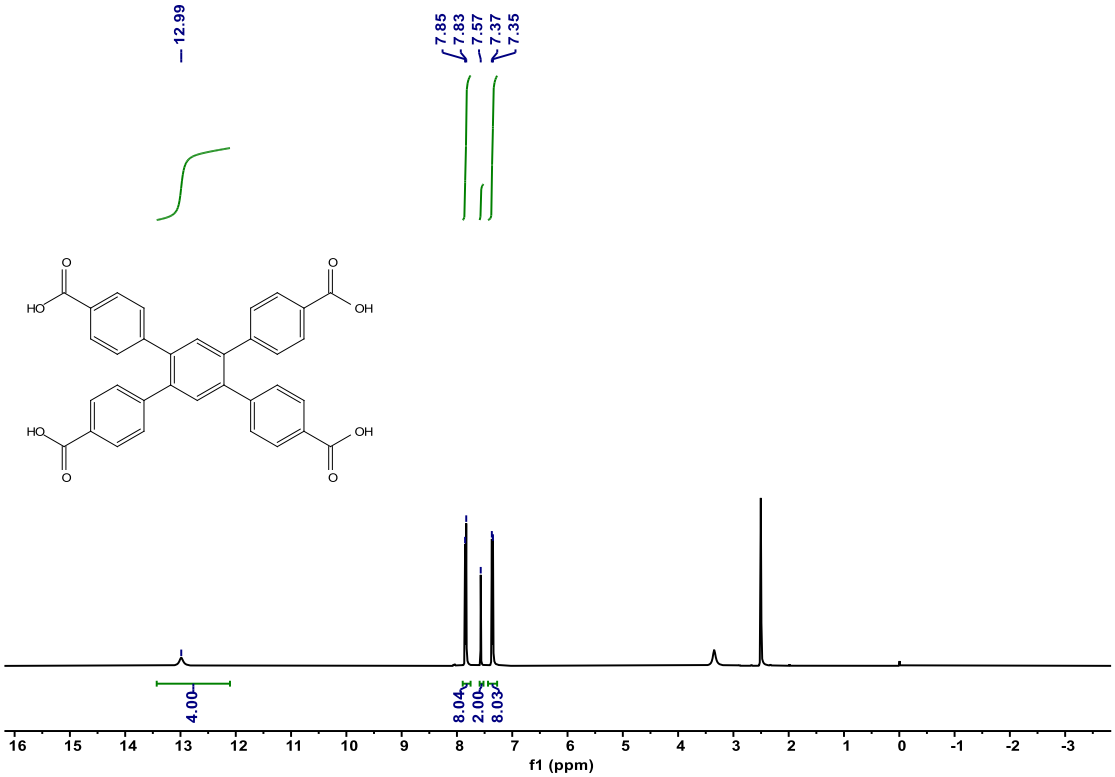

^{13}C NMR (100 MHz, DMSO) spectrum of H_4BTEB.

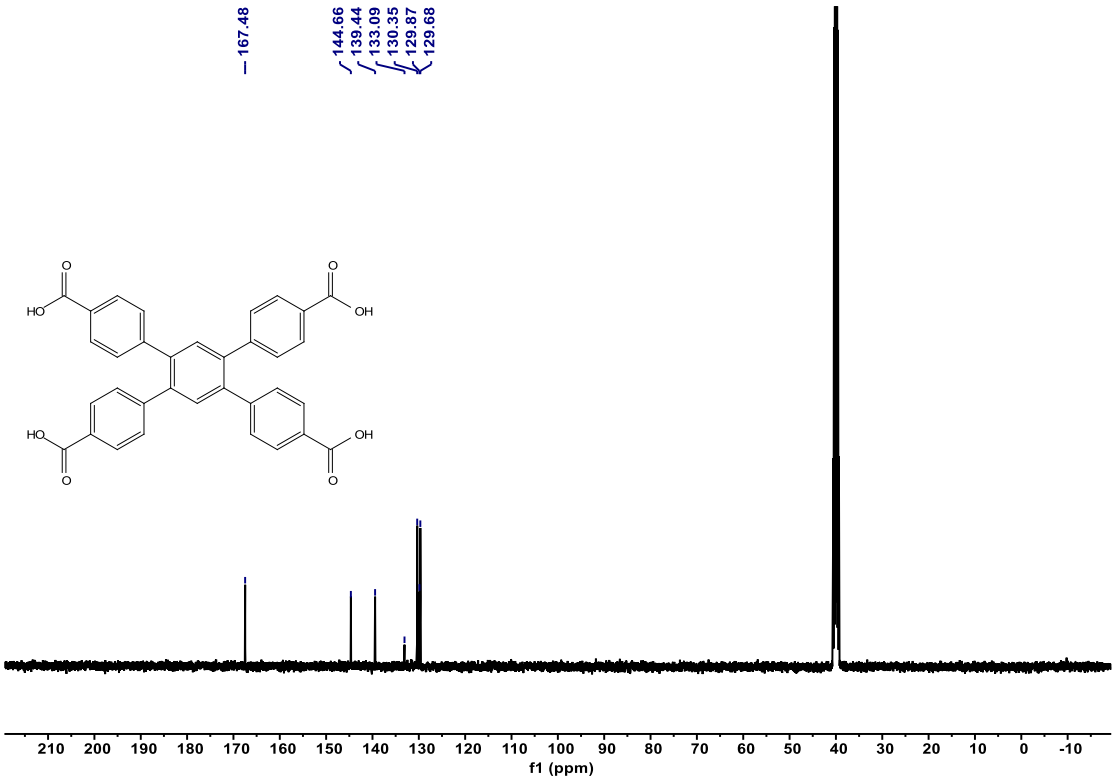

^{1}H NMR (400 MHz, $CDCl_3$) spectrum of intermediate E.

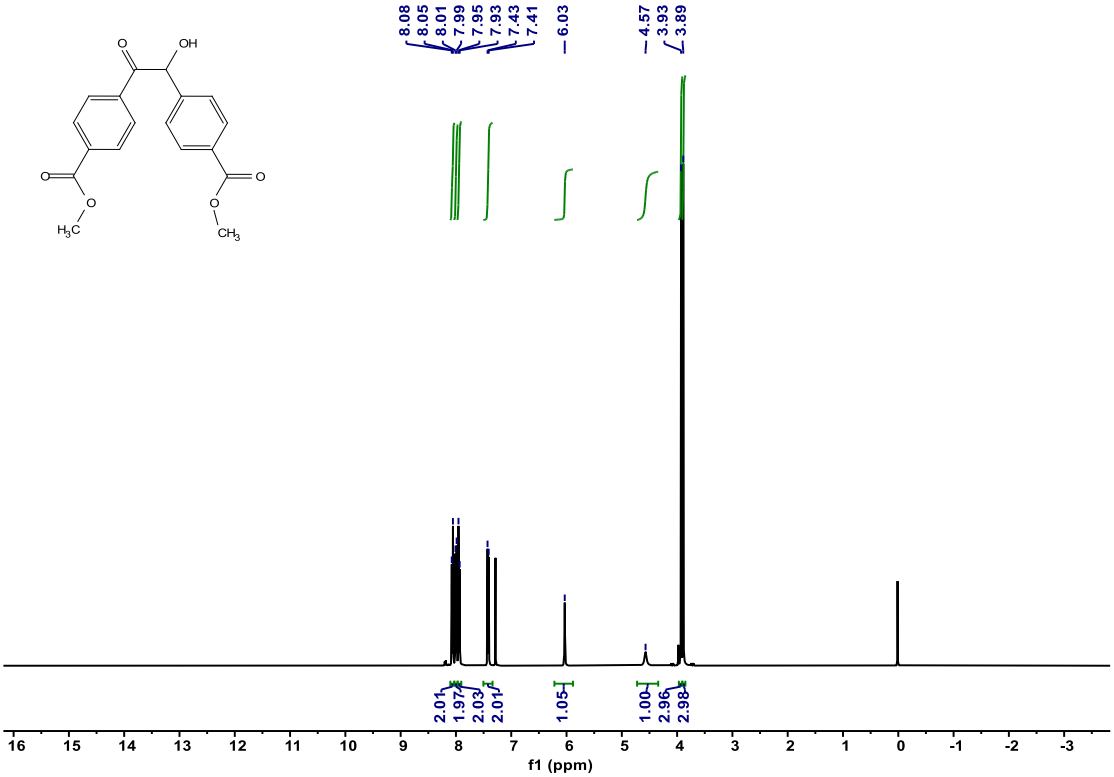

^{13}C NMR (100 MHz, $CDCl_3$) spectrum of intermediate E.

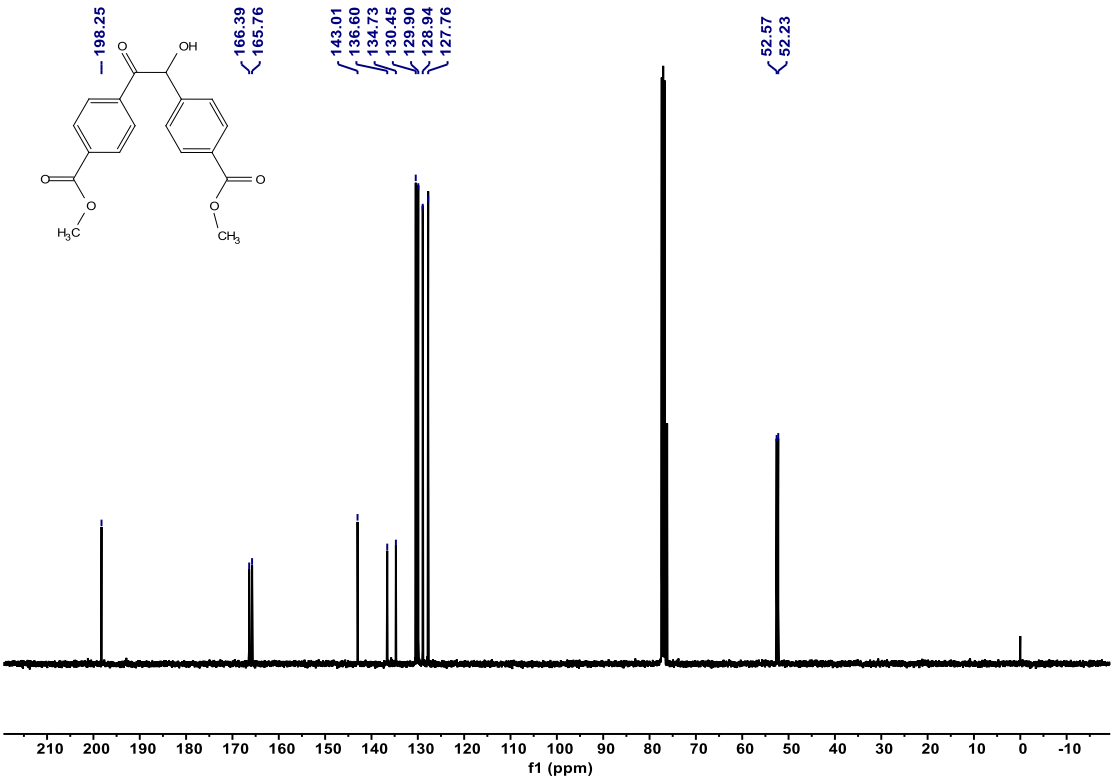

^{1}H NMR (400 MHz, $CDCl_3$) spectrum of intermediate F.

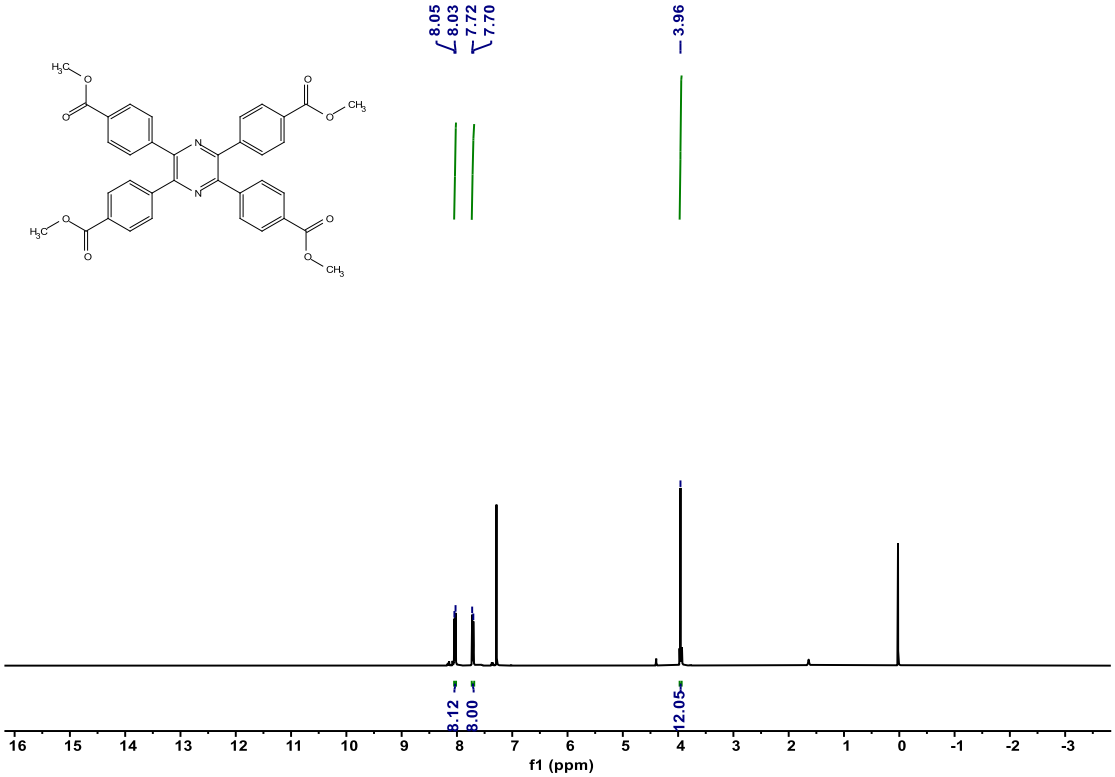

^{13}C NMR (100 MHz, $CDCl_3$) spectrum of intermediate F.

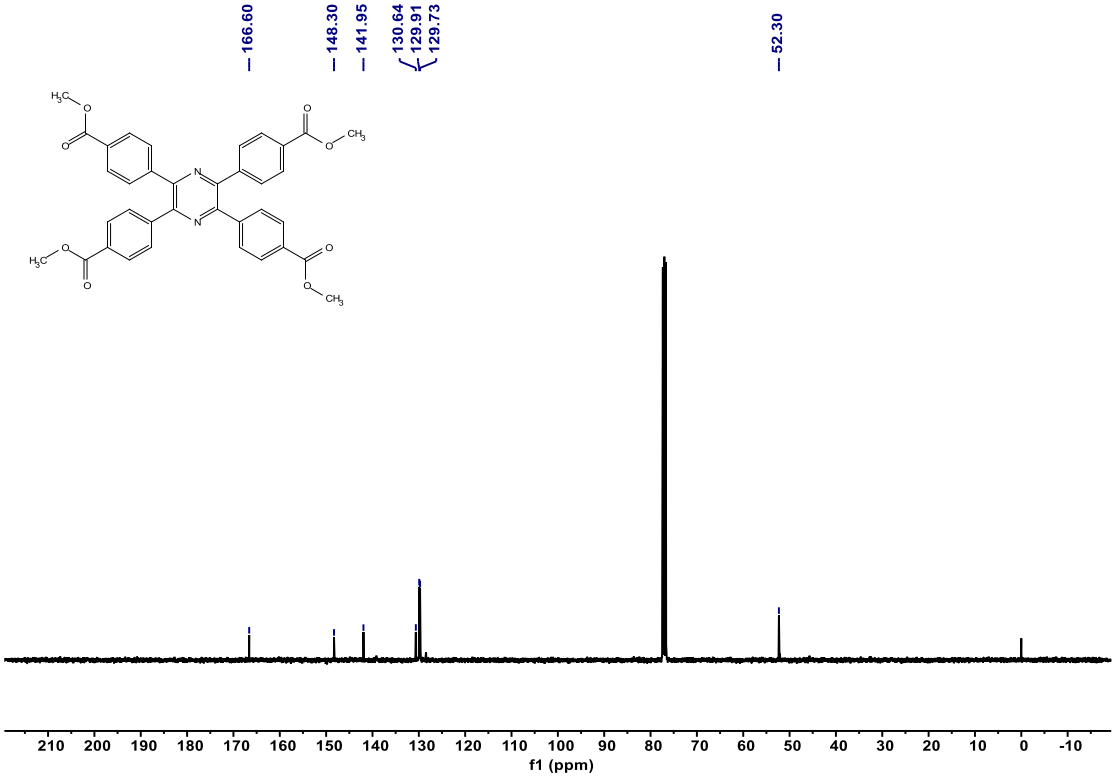

^{1}H NMR (400 MHz, $CDCl_3$) spectrum of H_4BTTB.

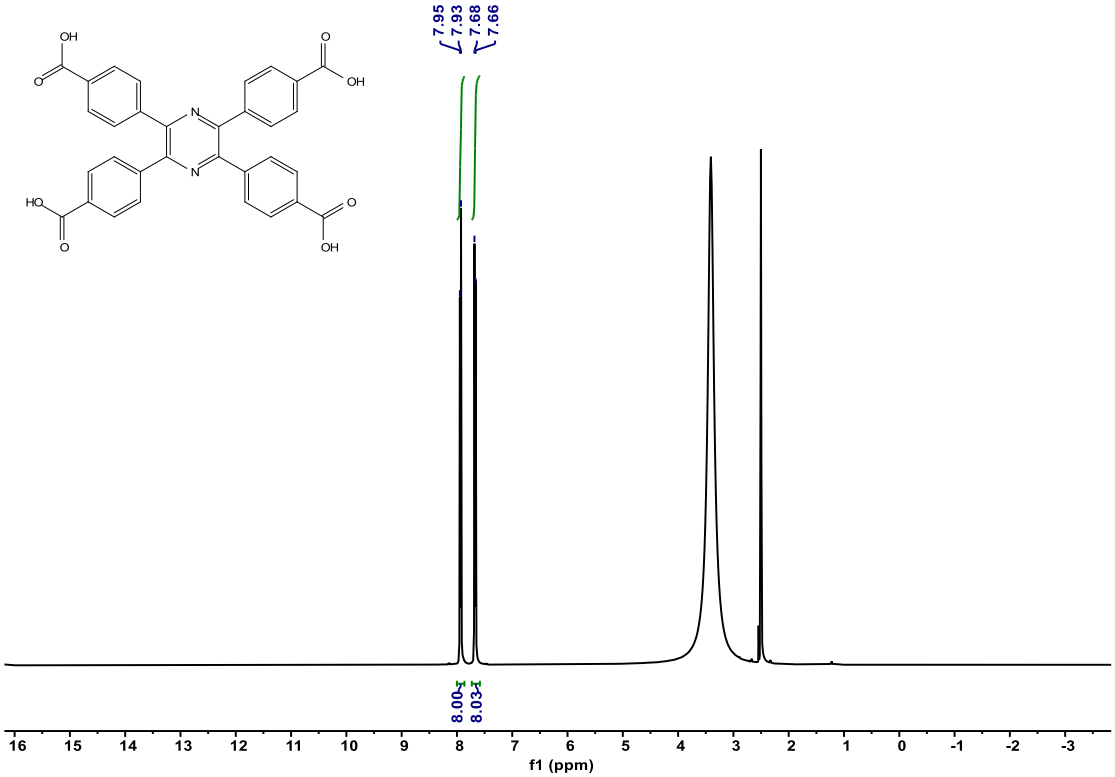

^{13}C NMR (100 MHz, DMSO) spectrum of H_4BTTB.

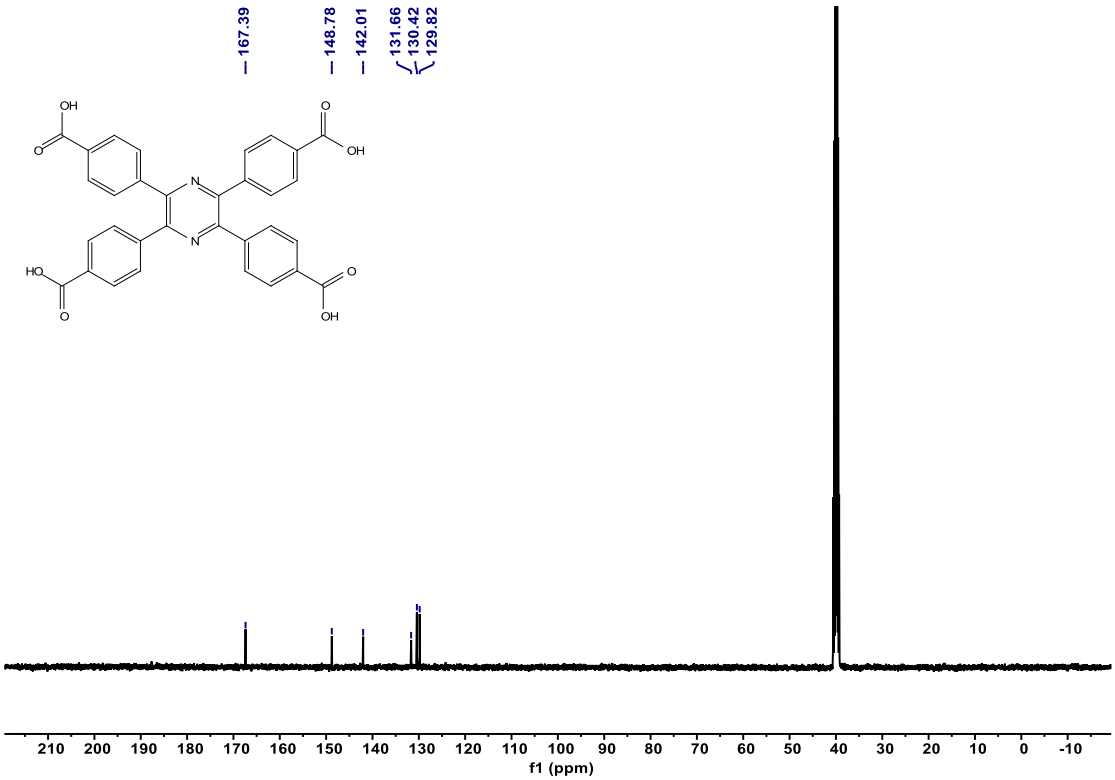

Reference

1. K. Wu, J. Zheng, Y.-L. Huang, D. Luo, Y. Y. Li, W. Lu and D. Li, *J. Mater. Chem. C*, 2020, **8**, 16974-16983.
2. K. Wu, Y.-L. Huang, J. Zheng, D. Luo, M. Xie, Y. Y. Li, W. Lu and D. Li, *Mater. Chem. Front.*, 2021, **5**, 4300-4309.
3. I. A. Ibarra, P. A. Bayliss, E. Pérez, S. Yang, A. J. Blake, H. Nowell, D. R. Allan, M. Poliakoff and M. Schröder, *Green Chem.*, 2012, **14**, 117-122.
4. Q. Liu, D. Ning, W. J. Li, X. M. Du, Q. Wang, Y. Li and W. J. Ruan, *Analyst*, 2019, **144**, 1916-1922.
5. Y. Zhou, Q. Yang, D. Zhang, N. Gan, Q. Li and J. Cuan, *Sens. Actuators, B,*, 2018, **262**, 137-143.
6. C. Li, C. Zeng, Z. Chen, Y. Jiang, H. Yao, Y. Yang and W. T. Wong, *J. Hazard. Mater.*, 2020, **384**, 121498.
7. X. Liu, Q. Ma, X. Feng, R. Li and X. Zhang, *Microchem. J.*, 2021, **170**, 106714.
8. C. Li, W. Yang, X. Zhang, Y. Han, W. Tang, T. Yue and Z. Li, *J. Mater. Chem. C*, 2020, **8**, 2054-2064.
9. Z. Gan, X. Hu, X. Xu, W. Zhang, X. Zou, J. Shi, K. Zheng and M. Arslan, *Food Chem.*, 2021, **354**, 129501.
10. Y. Q. Zhang, X. H. Wu, S. Mao, W. Q. Tao and Z. Li, *Talanta*, 2019, **204**, 344-352.
11. C. Li, L. Zhu, W. Yang, X. He, S. Zhao, X. Zhang, W. Tang, J. Wang, T. Yue and Z. Li, *J. Agric. Food. Chem.*, 2019, **67**, 1277-1283.
12. C. Li, X. Zhang, S. Wen, R. Xiang, Y. Han, W. Tang, T. Yue and Z. Li, *J. Hazard. Mater.*, 2020, **395**, 122615.
13. Y. Zhao, Q. Wang, H. Wang, H. Zhangsun, X. Sun, T. Bu, Y. Liu, W. Wang, Z. Xu and L. Wang, *Sens. Actuators, B,*, 2021, **334**, 129610.
14. Z. Gan, W. Zhang, J. Shi, X. Xu, X. Hu, X. Zhang, X. Wang, M. Arslan, J. Xiao and X. Zou, *Dyes and Pigments*, 2021, **194**.
15. N. Wu, H. Guo, M. Wang, Y. Cao, L. Sun, F. Yang, T. Zhang, L. Peng, Y. Liu and W. Yang, *Anal. Chim. Acta*, 2022, **1190**, 339247.
16. H.-H. Wang, Y. Zhang, D.-B. Yang, L. Hou, Z.-Y. Li and Y.-Y. Wang, *Cryst. Growth Des.*, 2021, **21**, 2488-2497.
17. T. Sun, R. Fan, J. Zhang, M. Qin, W. Chen, X. Jiang, K. Zhu, C. Ji, S. Hao and Y. Yang, *ACS Appl. Mater. Interfaces*, 2021, **13**, 35689-35699.
18. L. Yu, H. Chen, J. Yue, X. Chen, M. Sun, H. Tan, A. M. Asiri, K. A. Alamry, X. Wang and S. Wang, *Anal. Chem.*, 2019, **91**, 5913-5921.
19. G. Bussi, D. Donadio and M. Parrinello, *J. Chem. Phys.*, 2007, **126**, 014101.
20. F. Weigend, *Phys. Chem. Chem. Phys.*, 2006, **8**, 1057-1065.
21. G. W. T. H. B. S. G. E. S. M. A. R. J. R. C. G. S. V. B. B. M. M. J. Frisch and D. J. Fox, *Gaussian 09, Inc. Wallingford CT*, 2009.